

21 **Abstract**

22 Cellular differentiation is associated with the acquisition of a unique protein signature
23 which is essential to attain the ultimate cellular function and activity of the differentiated cell.
24 This is predicted to result in unique biosynthetic demands that arise during differentiation. Using
25 a bioinformatic approach, we discovered osteoblast differentiation is associated with increased
26 demand for the amino acid proline. When compared to other differentiated cells, osteoblast-
27 associated proteins including RUNX2, OSX, OCN and COL1A1 are significantly enriched in
28 proline. Using a genetic and metabolomic approach, we demonstrate that the neutral amino acid
29 transporter SLC38A2 acts cell autonomously to provide proline to facilitate the efficient
30 synthesis of proline-rich osteoblast proteins. Genetic ablation of SLC38A2 in osteoblasts limits
31 both osteoblast differentiation and bone formation in mice. Mechanistically, proline is primarily
32 incorporated into nascent protein with little metabolism observed. Collectively, these data
33 highlight a requirement for proline in fulfilling the unique biosynthetic requirements that arise
34 during osteoblast differentiation and bone formation.

35

36

37

38

39

40

41

42

43

44 **Background**

45

46 The mammalian boney skeleton is a remarkable organ that has multiple functions
47 including support, mobility, protection of internal organs, endocrine signaling, mineral storage as
48 well as being a site for red blood cell production (Guntur & Rosen, 2012; Jagannathan-Bogdan &
49 Zon, 2013; Long, 2012; Salhotra, Shah, Levi, & Longaker, 2020). The skeleton develops
50 embryonically through two distinct mechanisms, intramembranous and endochondral
51 ossification (Berendsen & Olsen, 2015). Intramembranous ossification is responsible for
52 forming the ‘flat’ bones of the skull. Here, mesenchymal progenitor cells condense and give rise
53 to bone directly. The remainder of the skeleton develops through endochondral ossification. In
54 this process, the mesenchymal progenitors condense and give rise to a cartilaginous template
55 which is subsequently ossified. Regardless of the developmental mechanism, skeletal
56 development depends upon osteoblasts. Osteoblasts are secretory cells responsible for producing
57 and secreting the Collagen Type 1 (COL1A1) rich extracellular bone matrix. Osteoblast
58 differentiation is tightly regulated by the transcription factors RUNX2 and OSX (encoded by *Sp7*)
59 (Ducy, Zhang, Geoffroy, Ridall, & Karsenty, 1997; Nakashima et al., 2002; Otto et al., 1997;
60 Takarada et al., 2016). Genetic studies in mice demonstrate RUNX2 is essential for commitment
61 to the osteoblast lineage as well as the transcriptional regulation of osteoblast marker genes (e.g.,
62 *Spp1* and *Bglap*) (Komori et al., 1997; Meyer, Benkusky, Lee, & Pike, 2014; Otto et al., 1997;
63 Wu et al., 2014). OSX functions downstream of RUNX2 to regulate osteoblast differentiation
64 and osteoblast gene expression (e.g., *Spp1*, *Ibsp*, and *Bglap*) (Bianco, Fisher, Young, Termine, &
65 Robey, 1991; Ducy et al., 1996).

66 During differentiation, osteoblasts acquire a distinct protein profile in addition to
67 increasing bone matrix production (Alves et al., 2010; A. X. Zhang et al., 2007). Protein and

68 bone matrix production is biosynthetically demanding and predicted to present differentiating
69 osteoblasts with changing metabolic demands (Buttgereit & Brand, 1995). Thus, osteoblasts
70 must maximize nutrient and amino acid acquisition for differentiation and matrix production to
71 proceed. Consistent with this, both glucose and amino acid uptake are required for osteoblast
72 differentiation and bone formation (Elefteriou et al., 2006; Rached et al., 2010; Wei et al., 2015).
73 Osteoblasts primarily rely on glycolytic metabolism of glucose which provides ATP for protein
74 synthesis and to regulate RUNX2 stability to promote osteoblast differentiation (Esen et al., 2013;
75 W.-C. Lee, Ji, Nissim, & Long, 2020; Wei et al., 2015). Like glucose, amino acids have long
76 been recognized as important regulators of osteoblast differentiation and bone matrix production
77 (Elefteriou et al., 2006; Hahn, Downing, & Phang, 1971; Karner, Esen, Okunade, Patterson, &
78 Long, 2015; Rached et al., 2010; Shen, Sharma, Yu, Long, & Karner, 2021; Yu et al., 2019).
79 Affecting the ability of cells to sense or obtain amino acids either by limiting their availability in
80 the media or inhibiting cellular uptake has detrimental effects on osteoblast differentiation and
81 bone formation (Chen & Long, 2018; Elefteriou et al., 2006; Esen et al., 2013; Hu et al., 2020;
82 Karner et al., 2015; Rached et al., 2010; Shen et al., 2021; Yu et al., 2019). Despite this, the role
83 of individual amino acids in osteoblasts is not well understood. Recent studies identified
84 glutamine as a particularly important amino acid in osteoblasts supporting protein and amino
85 acid synthesis, redox regulation and energetics (Karner et al., 2015; Shen et al., 2021; Stegen et
86 al., 2020; Yu et al., 2019). Whether other individual amino acids are similarly important for
87 osteoblast differentiation remains unknown.

88 Proline is an intriguing amino acid in osteoblasts as it is important for both the
89 biosynthesis and structure of collagen (Grant & Prockop, 1972; Krane, 2008). In addition,
90 interest in proline has recently increased as proline is critical for cancer cell survival,

91 tumorigenesis and metastasis (Liu, Glunde, et al., 2012; Nagano et al., 2017; Phang, Liu,
92 Hancock, & Christian, 2012). Proline is a multifunctional amino acid with important roles in
93 carbon and nitrogen metabolism, oxidative stress protection, cell signaling, nutrient adaptation
94 and cell survival (Hollinshead et al., 2018; Liu, Le, et al., 2012; Phang, 2019). Proline can
95 contribute to protein synthesis directly through incorporation into protein or can be metabolized
96 into downstream products involved in energetic and biosynthetic reactions. Despite its emerging
97 role in cancer cells, the role of proline during osteoblast differentiation and bone development is
98 understudied.

99 Here we identify proline as a critical nutrient in osteoblasts. Using a multifaceted
100 approach, we demonstrate that sodium-dependent neutral amino acid transporter-2 (SNAT2,
101 encoded by *Slc38a2* and denoted herein as SLC38A2) acts cell autonomously to provide proline
102 necessary for osteoblast differentiation and bone development. Mechanistically, proline is
103 essential for the synthesis of proline-rich osteoblast proteins including those that regulate
104 osteoblast differentiation (e.g., RUNX2 and OSX) and bone matrix production (e.g., COL1A1).
105 These data highlight a broad requirement for proline to fulfill unique synthetic demands
106 associated with osteoblast differentiation and bone formation.

107

108

109 **Results**

110 **Proline is enriched in osteoblast-associated proteins, leading to increased proline demand** 111 **during osteoblast differentiation.**

112 To identify if there are unique requirements for individual amino acids that arise during
113 differentiation, we first profiled the amino acid composition of select proteins (e.g., RUNX2,
114 OSX, COL1A1 and OCN) that are induced during osteoblast differentiation (Figure 1
115 Supplement 1). These classical osteoblast proteins are enriched with the amino acid proline and
116 to a lesser extent alanine when compared to all proteins (Figure 1A and Table 1). For
117 comparison, other amino acids were either uniformly underrepresented (e.g., Glu, Ile and Val) or
118 were enriched only in a subset of these proteins (e.g., Gly and Gln) (Figure 1A and Table 1). To
119 determine if this observation was characteristic of osteoblast proteins in general, we next
120 evaluated amino acid enrichment in proteins that are associated with osteoblast differentiation
121 based on gene ontology. Osteoblast-associated proteins (GO:0001649) were found to have a
122 higher proline composition when compared to the average of all proteins (7.1% vs 6.1% proline
123 for osteoblasts vs all proteins) (Table 2). In fact, many classical osteoblast proteins (e.g.,
124 RUNX2, OSX and COL1A1) were above the 90th percentile for proline composition and 43.5%
125 of all osteoblast proteins were above the 75th percentile for proline composition. No other amino
126 acids were similarly enriched in osteoblast-associated proteins (Table 2). Moreover, osteoblast-
127 associated proteins were enriched for proline when compared to proteins associated with other
128 cell types including osteoclasts (GO:0030855), cardiomyocytes (GO:0001649), muscle cells
129 (GO:0055007), hematopoietic stem cells (GO:0042692), endothelial cells (GO:0030182),
130 epithelial cells (GO:0055007) or neurons (GO:0030182) (Figure 1B and Table 2). In contrast,
131 alanine enrichment was comparable amongst the different cell types (Figure 1B and Table 2).

132 These data suggest that osteoblast differentiation is associated increased proline demand. To test
133 this hypothesis, we transcriptionally profiled naïve calvarial cells that were induced to undergo
134 osteoblast differentiation and quantified the proline enrichment of the encoded proteins.
135 Consistent with our previous analysis, proline was enriched in proteins encoded by the induced
136 genes compared to either all genes or genes that were suppressed in differentiated calvarial
137 osteoblasts (Figure 1C). Moreover, comparing the basal and differentiation associated
138 transcriptional changes with proline composition indicates that proline demand is predicted to
139 rise whereas alanine demand is predicted to decline during osteoblast differentiation (Figure 1D).
140 All together, these data predict proline is uniquely required during osteoblast differentiation due
141 to the increasing expression of proline-enriched osteoblast proteins.

142 We next sought to understand proline dynamics in osteoblasts. Proline can be taken up
143 from the extracellular milieu or synthesized. To determine the source of proline in osteoblasts,
144 we first performed stable isotopomer analysis using $^{13}\text{C}_\text{U}$ -Proline to evaluate proline uptake or
145 either $^{13}\text{C}_\text{U}$ -Glutamine or $^{13}\text{C}_{1,2}$ -Glucose to estimate *de novo* proline biosynthesis. 10.5% of
146 intracellular proline is synthesized from either glutamine (9.9%) or glucose (0.6%) in 24 hours
147 (Figure 2A). By comparison, 37.8% of the proline pool is labeled from $^{13}\text{C}_\text{U}$ -proline after 24
148 hours and this increased to 66.6% after 72 hours (Figure 2A). The slow labeling of proline when
149 compared to intracellular glutamine which reached saturation within hours, suggests that in naïve
150 calvarial cells, proline uptake is slow, and the intracellular proline pool is relatively stable with
151 little turnover. To test this, we performed radiolabeled amino acid uptake assays to compare the
152 rates of proline and glutamine uptake. Consistent with the labeling data, proline uptake was slow
153 compared to glutamine uptake in naïve cells (Figure 2B and Figure 2 Supplement 1A). During
154 differentiation, the rate of proline uptake increased significantly and to a greater extent than

155 glutamine which also increased (Figure 2C and Figure 2 Supplement 1B). The tracing
156 experiments indicated little proline metabolism occurs in osteoblasts as proline carbon was not
157 observed in any other amino acid or downstream metabolite even after 72 hours (Figure 2A). By
158 comparison, carbon from both glutamine and glucose was observed in many metabolites
159 including TCA cycle intermediates and amino acids (Figure 2A and not shown). These data
160 suggest proline is not metabolized and is primarily used for protein synthesis. Consistent with
161 this conclusion, proline incorporation into both total protein and collagen significantly increases
162 during differentiation (Figure 2D). Moreover, almost 50% of proline in total protein was derived
163 from $^{13}\text{C}_U$ -Proline (Figure 2E). Importantly, we observed no proline-derived amino acids in total
164 protein despite the presence of glutamine derived amino acids including proline (Figure 2E).
165 Thus, proline demand and protein synthesis rise concomitantly during osteoblast differentiation.

166 We next sought to determine the effects of proline withdrawal on protein expression.
167 Proline withdrawal specifically reduced charging of the proline tRNA (AGG) but did not affect
168 the activation of either the mTOR pathway (as determined by S6 ribosomal protein
169 phosphorylation at S235/236) or the integrated stress response (ISR) (as determined by and
170 EIF2a phosphorylation at Ser51) (Figure 3 Supplement 1A-B). Proline withdrawal did not affect
171 the expression of select non-proline enriched proteins (Figure 3A and Figure 3 Supplement 1B).
172 Conversely, proline withdrawal significantly reduced the expression of osteoblast proteins that
173 had higher than average proline content including COL1A1 (19.1% proline), RUNX2 (10.5%
174 proline), OSX (13.3% proline) and ATF4 (10.6% Proline) (Figure 3A). Importantly, proline
175 withdrawal did not affect the mRNA expression of these proteins (Figure 3 Supplement 1C). We
176 next took a candidate approach and evaluated other proline-enriched (e.g., EIF4EBP1 (13.7%
177 proline), PAX1 (11.1% proline), ATF2 (10.7% proline), SMAD1 (9.9% proline), and EIF2A,

178 (7.6% proline)) and non-enriched proteins (ERK1 (6.6% proline), PHGDH (5.3% proline), EEF2
179 (5.2% proline), AKT (4.6% proline), ACTB (5.1% proline), mTOR (4.4% proline), TUBA (4.4%
180 proline) and S6RP (4.2% proline)) that are not known to be required for osteoblast differentiation
181 but are expressed in calvarial cells according to our transcriptomic analyses. Proline withdrawal
182 significantly reduced the expression of the proline enriched proteins without affecting the low
183 proline proteins (Figure 3A and Figure 3 Supplement 1B). The reduction in protein expression
184 significantly correlated with the proline content in the proteins (Figure 3B). These data indicate
185 this phenomenon is broadly generalizable in osteoblasts. The decreased protein expression is
186 due primarily to reduced synthesis of proline enriched proteins as cycloheximide washout
187 experiments found proline withdrawal resulted in a significant delay in the recovery of proline-
188 enriched protein expression (Figure 3C and Figure 3 Supplement 1D-H). Thus, proline is
189 essential for the synthesis of proline-enriched osteoblast proteins.

190

191 **SLC38A2 provides proline to facilitate the synthesis of proline rich osteoblast proteins.**

192 We next sought to identify the proline transporter in osteoblasts. Proline uptake in
193 osteoblasts is reported to occur in a 2-(methylamino)-isobutyric acid (MeAIB) sensitive manner
194 (Baum & Shteyer, 1987; Yee, 1988). Consistent with these reports, MeAIB reduced proline
195 uptake by 80% in both osteoblasts and bone shafts with minimal effects on the uptake of other
196 amino acids (e.g., Gln, Ala, Gly or Ser) (Figure 4A and Figure 4 Supplement 1A). We next
197 sought to identify candidate proline transporters based on relative mRNA expression. Evaluation
198 of our transcriptomic data identified *Slc38a2* as the highest expressed putative proline transporter
199 in calvarial cells (Table 3). *Slc38a2* encodes the sodium-dependent neutral amino acid
200 transporter-2 (SNAT2, denoted here as SLC38A2) which transports neutral alpha amino acids

201 (e.g., proline) in a Na⁺ dependent manner that is sensitive to MeAIB (Grewal et al., 2009;
202 Hoffmann et al., 2018). To determine if SLC38A2 transports proline in differentiating
203 osteoblasts, we targeted *Slc38a2* using a CRISPR/Cas9 approach (Figure 4 Supplement 1B).
204 *Slc38a2* targeting significantly reduced SLC38A2 protein and reduced radiolabeled proline
205 uptake by ~50% in differentiated calvarial cells (Figure 4B-C). This is likely a slight
206 underestimation of SLC38A2 dependent proline uptake due to incomplete ablation of SLC38A2
207 protein (Figure 4C). Consistent with decreased proline uptake, *Slc38a2* ablation specifically
208 reduced proline-tRNA charging similar to proline withdrawal without negatively affecting
209 charging of other tRNAs or activating the ISR (Figure 4 Supplement 1C-D). Moreover, *Slc38a2*
210 ablation specifically reduced the expression of the proline enriched proteins without affecting the
211 expression of non-proline enriched proteins or mRNA expression of these proteins (Figure 4C
212 and Figure 4 Supplement 1D). The effect of *Slc38a2* ablation on protein expression significantly
213 correlated with the proline content in the proteins (Figure 4D). This is likely a direct result of
214 decreased proline uptake as *Slc38a2* deletion did not affect mTOR activation or induce ISR
215 (Figure 4 Supplement 1D). Thus, SLC38A2 provides proline for the efficient synthesis of
216 proline-enriched proteins.

217

218 **SLC38A2 provides proline necessary for bone development**

219 We next sought to understand the role of SLC38A2 during osteoblast differentiation.
220 *Slc38a2* deletion did not affect cell viability, proliferation, or the mRNA expression or induction
221 of early osteoblast regulatory genes (e.g., *Akp2* and *Runx2*) (Figure 5 Supplement 1A-C).
222 However, *Slc38a2* deficient cells were characterized by reduced induction of *Sp7* and terminal
223 osteoblast marker genes (e.g., *Ibsp* and *Bglap*) as well as reduced matrix mineralization (Figure 5

224 Supplement 1C-D). This indicates that SLC38A2 provides proline required for terminal
225 osteoblast differentiation and matrix mineralization *in vitro*.

226 In light of these data, we next analyzed the function of *Slc38a2* during osteoblast
227 differentiation by comparing mice null for SLC38A2 due to the insertion of LacZ into the coding
228 region of *Slc38a2* (*Slc38a2^{LacZ/LacZ}*). We verified the absence of SLC38A2 expression by
229 western blot (Figure 5 Supplement 2A). Using alcian blue and alizarin red staining (which stains
230 cartilage and bone matrix blue or red respectively) we found that *Slc38a2^{LacZ/LacZ}* embryos were
231 characterized by a conspicuous reduction in red mineralized bone matrix staining in both
232 endochondral and intramembranous bones at E15.5 (Figure 5A-B). This defect in bone
233 mineralization was most obvious in the developing skull (Figure 5B). By comparison,
234 *Slc38a2^{LacZ/LacZ}* animals had no apparent defects in cartilage formation at E15.5 indicating loss of
235 *Slc38a2* impacts osteoblast differentiation. To test this, we crossed mice harboring a floxed
236 allele of *Slc38a2* (*Slc38a2^{fl}*) with mice expressing Cre recombinase under the control of the *Sp7*
237 promoter (*Sp7Cre*) which is active in osteoblast progenitors beginning at E14.5 (Rodda &
238 McMahon, 2006). *Sp7Cre;Slc38a2^{fl/fl}* bones were characterized by reduced SLC38A2
239 expression and reduced proline uptake (Figure 5 Supplement 3A-B). Like the *Slc38a2^{LacZ/LacZ}*
240 mice, *Sp7Cre;Slc38a2^{fl/fl}* mice had significantly less alizarin red stained bone matrix at E15.5
241 (Figure 5C-D). By postnatal day 1 (P1), overall bone matrix in long bones was comparable in
242 both genetic models, however the skulls from both *Slc38a2^{LacZ/LacZ}* and *Sp7Cre;Slc38a2^{fl/fl}* mice
243 continued to be poorly mineralized with patent fontanelles compared to their respective
244 littermate controls (Figure 5E-H, Figure 5 Supplement 3C). Because we observed a consistent
245 defect in intramembranous ossification and *Sp7Cre* is expressed in both osteoblasts and
246 hypertrophic chondrocytes in the developing limbs we focused our molecular analyses on the

247 osteoblasts in the developing calvarium. *Sp7Cre;Slc38a2^{fl/fl}* calvariae had normal alkaline
248 phosphatase staining despite less mineralized area shown by von Kossa staining (Figure 5I-L).
249 The defects in bone development are attributed to delayed osteoblast differentiation as
250 *Sp7Cre;Slc38a2^{fl/fl}* mice had significantly reduced expression of *Spp1*, *Ibsp* and *Bglap* (Figure
251 5M-R). This was not due to a reduction in overall osteoblast numbers as there was no difference
252 in the total number of *Sp7:GFP* expressing cells per mineralized area (Figure 5S-T). Despite this,
253 significantly fewer *Sp7:GFP* expressing cells were found to have OSX (encoded by *Sp7*) or
254 RUNX2 protein expression in *Sp7Cre;Slc38a2^{fl/fl}* animals (Figure 5S-T and Figure 5 Supplement
255 3C). Similar results were observed in the limbs of both *Slc38a2^{LacZ/LacZ}* and *Sp7Cre;Slc38a2^{fl/fl}*
256 mice at E15.5 (Figure 5 Supplements 2B and 3D). Similarly, *Sp7GFP* expressing cells in
257 *Sp7Cre;Slc38a2^{fl/fl}* mice had significantly reduced COL1A1 protein expression despite normal
258 *Colla1* mRNA expression when compared to *Sp7Cre;Slc38a2^{fl/+}* controls (Figure 5U-X and
259 Figure 5 Supplement 2B and 3C). For comparison, the expression of proline poor Actin (as
260 determined by phalloidin staining) and GFP (4.2% Proline) were unaffected in
261 *Sp7Cre;Slc38a2^{fl/fl}* calvariae (Figure 5 Supplement 3C). Collectively these data indicate *Slc38a2*
262 provides proline essential for osteoblast differentiation and bone formation during bone
263 development.

264

265

266

267

268

269 **Discussion**

270

271 Here we have defined the major role for proline during osteoblast differentiation and

272 bone formation. Namely, that osteoblasts require proline to fulfill unique biosynthetic demands

273 that arise due to increased production of proline enriched osteoblast-associated proteins.

274 Consistent with this, osteoblasts significantly increase proline consumption and to a lesser extent

275 proline biosynthesis during differentiation. Genetically limiting proline uptake by ablating the

276 proline transporter SLC38A2 results in delayed bone development and decreased bone mass in

277 adult male mice. Mechanistically, osteoblasts utilize proline primarily for the synthesis of

278 proline enriched osteoblast proteins to facilitate both osteoblast differentiation and bone matrix

279 production. Collectively, these data highlight a broad requirement for proline to regulate

280 osteoblast differentiation and bone development in addition to supporting collagen synthesis.

281 Osteoblast differentiation is characterized by a distinct protein profile in addition to

282 increasing bone matrix production (Alves et al., 2010; A. X. Zhang et al., 2007). These

283 osteoblast-associated proteins are enriched for the amino acid proline compared to all other

284 proteins (Figure 1 and Tables 1-2). We and others have recently described increased

285 consumption of numerous amino acids in differentiating osteoblasts including glutamine

286 (Sharma, Yu, Shen, Zhang, & Karner, 2021; Stegen et al., 2020; Yu et al., 2019), asparagine

287 (Sharma et al., 2021) and proline (this study). Glutamine and asparagine contribute to both *de*

288 *novo* amino acid biosynthesis and protein synthesis directly (Sharma et al., 2021). Our data here

289 indicates the primary use for proline is direct incorporation into nascent protein. Consistent with

290 this, reducing proline availability specifically reduced the synthesis of proteins with higher-than-

291 average proline content without affecting mTOR activation or inducing ISR (Figures 3 and 4).

292 In fact, protein expression was negatively correlated with the proline content in proteins when

293 proline availability or uptake was limited (Figure 3 and 4). By comparison, limiting the
294 availability of glutamine induced robust activation of the ISR and inhibits global protein
295 synthesis (Sharma et al., 2021). This likely reflects the necessity of glutamine metabolism to
296 maintain amino acid concentrations (including proline) and provide other metabolites during
297 osteoblast differentiation (Sharma et al., 2021; Stegen et al., 2020; Yu et al., 2019). Consistent
298 with the more direct use of proline in protein but not amino acid biosynthesis, we did not observe
299 activation of the ISR in proline free conditions despite reduced charging of proline tRNA. It is
300 important to note that we evaluated the effects of proline withdrawal for 48 hours. This time
301 point may miss the chronic effects of proline withdrawal as proline uptake is slow and the
302 intracellular proline pool is stable with low turnover in naïve calvarial cells (Figure 2). Under
303 these conditions, *de novo* biosynthesis of proline may be sufficient to meet the basal needs of
304 naïve calvarial cells. Regardless, proline removal results in reduced synthetic efficiency of
305 proline-rich proteins. This effect is likely exacerbated during osteoblast differentiation as these
306 proline-rich proteins are increased.

307 Previous studies characterized proline uptake in both bones and osteoblasts directly.
308 These studies described proline uptake occurring primarily via System A but did not identify
309 individual transporters mediating proline uptake (Adamson & Ingbar, 1967; Finerman &
310 Rosenberg, 1966; Hahn, Downing, & Phang, 1969; Yee, 1988). Here, we identified the sodium-
311 dependent neutral amino acid transporter SLC38A2 as responsible for approximately 55% of
312 proline uptake in both calvarial osteoblasts and isolated bones (Figure 4B and Figure 5
313 Supplement 3B). This is consistent with previous reports that System A mediates 60% of proline
314 uptake in osteoblasts (Yee, 1988). Interestingly, SLC38A2 ablation affected only proline uptake
315 (Figure 5 Supplement 3B). It is not clear why SLC38A2 exclusively transports proline in

316 osteoblasts as amino acid transporters are thought to be promiscuous in their substrate specificity
317 (Kandasamy, Gyimesi, Kanai, & Hediger, 2018; Teichmann et al., 2017). For example,
318 SLC38A2 is reported to transport alanine, serine, glycine and glutamine in different cellular
319 contexts (Bröer, Rahimi, & Bröer, 2016; Morotti et al., 2019). Our data indicates glutamine is
320 not a primary substrate for SLC38A2 in bone cells. This is consistent with our recent data
321 demonstrating glutamine uptake is mediated primarily by System ASC with no involvement of
322 System A in osteoblasts (Sharma et al., 2021; Shen et al., 2021) . In light of these data, a better
323 understanding of the molecular regulation of SLC38A2 activity and substrate specificity is
324 needed. In addition, it will be important to identify the transporters mediating SLC38A2
325 independent proline uptake as well as to understand their function during osteoblast
326 differentiation and bone development.

327 Reducing proline uptake inhibited bone development in mice (Figure 5). This phenotype
328 was attributed primarily to decreased osteoblast differentiation and reduced bone matrix
329 production. Osteoblast differentiation and bone matrix production are associated with a unique
330 biosynthetic demand for proline. Using a bioinformatic approach, we discovered that osteoblast
331 associated proteins are more enriched for proline than any other amino acid when compared to
332 other cell types, (Figure 1). Many of these proline-rich proteins are essential regulators of
333 osteoblast differentiation (e.g. RUNX2, OSX and ATF4), bone matrix production (e.g., COL1A1)
334 or regulate the endocrine functions of bone (e.g., OCN) (Ducy et al., 1996; Ducy et al., 1997;
335 Elefteriou et al., 2006; Kern, Shen, Starbuck, & Karsenty, 2001; Nakashima et al., 2002; Otto et
336 al., 1997; Yang et al., 2004). Limiting proline availability by genetically ablating SLC38A2
337 specifically affected the production of proline rich proteins (e.g., RUNX2, OSX and COL1A1) in
338 a manner that was proportional to the relative proline content. It is important to note that

339 relatively minor reductions in protein expression or function are known to negatively impact
340 osteoblast differentiation and bone development and underly human bone diseases (Baek et al.,
341 2013; Bardai et al., 2016; Ben Amor, Roughley, Glorieux, & Rauch, 2013; Choi et al., 2001;
342 Lapunzina et al., 2010; B. Lee et al., 1997; Lou et al., 2009; Mundlos et al., 1997; S. Zhang et al.,
343 2009). Thus, ablating SLC38A2 dependent proline uptake has broad effects on osteoblast
344 differentiation due to minor reductions in many proline-rich osteoblast regulatory proteins. This
345 highlights an unappreciated mechanism by which osteoblast differentiation is responsive to
346 nutrient (e.g., proline) availability. When proline is available, osteoblast progenitors efficiently
347 synthesize the proline rich proteins necessary for differentiation (RUNX2 and OSX) and bone
348 matrix deposition (COL1A1). The high proline content of these proteins presents a novel
349 cellular checkpoint to ascertain if appropriate resources, in this case proline, are available for
350 osteoblast differentiation to proceed. When proline is limited, these proteins are not efficiently
351 synthesized which limits osteoblast differentiation and bone matrix production until sufficient
352 proline is available. This is critical to ensure cells can meet the synthetic challenges associated
353 with osteoblast differentiation and bone matrix production.

354 In summary, we have defined the necessity and the molecular substrates of *Slc38a2* in
355 osteoblasts. Our data indicates that SLC38A2 acts cell autonomously in osteoblasts to provide
356 proline and that SLC38A2 is the major proline transporter in osteoblasts. Proline is essential for
357 the production of proline-rich transcription factors (e.g., RUNX2 and OSX) and matrix proteins
358 (COL1A1) necessary for osteoblast differentiation and bone formation. These data expand our
359 understanding of the regulation of proline uptake and usage in osteoblasts and underscore the
360 necessity of proline for osteoblast differentiation and bone development.

361

362 **Materials and Methods**

363 **Mouse strains**

364 *C57Bl/6J* (RRID: IMSR_JAX:000664), *Rosa26Cas9* (RRID: IMSR_JAX:024858), *Rosa26FLP*
365 (RRID: IMSR_JAX:003946) and *Sp7-tTA,tetO-EGFP/Cre* (RRID: IMSR_JAX:006361) mouse
366 strains were obtained from the Jackson Laboratory. *Slc38a2LacZ* (C57BL/6N-
367 A<tm1Brd>Slc38a2<tm1a(KOMP)Wtsi>/Wtsi Ph) was purchased from the European Mouse
368 Mutant Archive (www.emmanet.org). To generate *Slc38a2^{fllox}*, *Slc38a2^{LacZ}* mice were crossed to
369 *Rosa26FLP* to remove FRT-flanking LacZ cassette followed by a backcrossing with *C57Bl/6J* to
370 remove *Rosa26^{FLP}* allele. Mice were housed at 23 °C on a 12-hour light/dark cycle with free
371 access to water and PicoLab Rodent Diet 20 (LabDiet #5053, St. Louis, MO). All mouse
372 procedures were approved by the Animal Studies Committees at Duke University first and then
373 the University of Texas Southwestern Medical Center at Dallas.

374 **Mouse analyses**

375 Skeletal preparations were performed on embryonic day (E) 15.5 or postnatal (P) day 0 embryos
376 obtained from timed pregnancies. Noon of the day of plugging was considered 12 hours post
377 coitum or E0.5. Embryos are dehydrated in 95% ethanol overnight followed by submersion in
378 acetone overnight. Specimens were then stained with 0.03% alcian blue in 70% ethanol and
379 0.005% alizarin red in water overnight. Stained embryos were then cleared in 1% KOH prior to a
380 graded glycerol series (30%, 50% and 80%). For histological analyses, freshly isolated limbs or
381 calvariae were fixed in 4% PFA at 4°C overnight. Limbs were then processed and embedded in
382 paraffin and sectioned at 5µm using a Microtome (Leica RM2255). Calvariae were cryoprotected
383 in 30% sucrose overnight, embedded in OCT and sectioned at 10µm using a Cryostat (Leica
384 CM1950).

385 ***In Situ* hybridization**

386 *In situ* hybridization was performed on 10µm cryosectioned calvariae or 5µm paraffin-sectioned
387 limbs. Cryosections were washed with water first for 5min. Paraffin sections were
388 deparaffinized and rehydrated, followed by 20mg/ml proteinase K treatment for 10min. Sections
389 were first then fixed in 4%PFA for 10min followed by 10 min acetylation. Sections were then
390 incubated in hybridization buffer for 2 hours at room temperature. Digoxigenin-labeled
391 antisense RNA probes for *Colla1* (HindIII, T7), *Sp7* (NotI, T3), *Spp1* (EcoRI, SP6), *Ibsp* (NOTI,
392 SP6) or *Bglap* (XbaI, T3) were hybridized at 60 °C overnight.

393 **Immunohistochemistry**

394 Sections were blocked in 1.5% goat serum in PBST and incubated with the following primary
395 antibodies (1:250 in blocking solution) as indicated: Anti-Coll1a1 (AB_1672342), Anti-Osx
396 (AB_2194492) or Anti-Runx2 (AB_10949892) at 4 °C overnight. Sections were then incubated
397 with Alexa Fluor 568 goat anti-rabbit (AB_143157)/-mouse IgG(H+L) antibody (AB_2534072)
398 at 1:250 dilution at room temperature for 30min. Sections were post fixed in 4% PFA for 10 min
399 before mounting. For actin staining, Alexa Fluor 647 Phalloidin (Invitrogen; 1:200 in blocking
400 buffer) was applied to sections before mounting. Sections were mounted using Heatshield with
401 DAPI (Vector).

402 **Cell culture**

403 Primary calvarial osteoblasts were isolated as follows. The calvaria of P4 pups were harvested
404 and extemporaneous tissue was removed. The calvariae was chopped by scissor into small pieces
405 and washed with PBS twice. The calvaria pieces were then incubated in 1.8mg/mL Collagenase
406 P in PBS for 10 minutes with agitation at 37°C four times. The first digestion was discarded, and
407 the last three digestions were collected and run through 70 µm cell strainer. Cells were then

408 centrifuged at 350x g for 5min and cultured at T75 flasks in aMEM containing 15% FBS at 37 °C
409 and 5% CO₂. Cells were plated at 1x10⁵ cells/mL for further experiments when it reached 90%
410 confluency. Osteoblast differentiation was induced at 100% confluency using aMEM
411 supplemented with 50 mg/ml ascorbic acid and 10 mM β-glycerophosphate for the indicated
412 time with a change of media every 48 hours. For proline drop out experiments, primary calvarial
413 cells were treated with proline-free aMEM (Genaxxon) supplemented back to 0.3mM proline or
414 not for the indicated length of time. To evaluate the synthesis of individual proteins,
415 cycloheximide (CHX) washout experiments were performed. Calvarial osteoblasts were treated
416 with 10μg/mL CHX for 24 hours. Cells were then chased with aMEM containing either 0.3mM
417 or 0mM proline for up to 24h before proteins were harvested. Alkaline phosphatase activity was
418 assessed using 5-bromo-4-chloro-3'-indolyphosphate/nitro blue tetrazolium (BCIP/NPT).
419 Mineralization was visualized by either von Kossa or Alizarin Red staining as indicated.

420

421 **CRISPR/Cas9 targeting**

422 Lentiviral vectors expressing single guide RNAs (sgRNA) targeting either *Slc38a2* or Luciferase
423 and mCherry were cloned into the LentiGuide-Puro plasmid according to the previously
424 published protocol (Sanjana, Shalem, & Zhang, 2014). The LentiGuide-Puro plasmid was a gift
425 from Feng Zhang (Addgene plasmid #52963). Sequences of each sgRNA protospacer are shown
426 in Table S1. To make viral particles, the sgRNA carrying lentiviral vector was cotransfected in
427 293T cells with the plasmids pMD2.g and psPax2. Virus containing media was collected and run
428 through 0.45 μm filter. Calvarial osteoblasts harvested from *Rosa26^{Cas9/Cas9}* pups were infected
429 for 24 hours and recovered for 24h in regular media before further experiments.

430

431 **Mass spectrometry**

432 Calvarial osteoblasts were cultured in 6cm plates until confluency before sample preparation for
433 mass spectrometry. For glucose, glutamine and proline tracing experiments, naïve or
434 differentiated calvarial cells were cultured in aMEM (Genaxxon) containing 0.3mM [U-¹³C]-
435 Proline (Cambridge), 2mM [U-¹³C]-Glutamine (Cambridge) or 5.6mM [1,2-¹³C]-Glucose
436 (SigmaAldrich) for 24h or 72h. The labeling was terminated with ice cold PBS and cells were
437 scrapped with -20°C 80% methanol on dry ice. 20nmol norvaline was added into each methanol
438 extract as internal control, followed by centrifuge at 10000 x g for 15 minutes. Supernatants were
439 processed and analyzed by the Metabolomics Facility at the Children’s Medical Center Research
440 Institute at UT Southwestern. For tracing experiments into protein, cells were labeled for 0, 12,
441 24 or 72 hours. Cell were then scrapped in 1M perchloric acid. The protein pellet was washed
442 with 70% ethanol three times. The pellet was then incubated with 1mL of 6M HCl at 110 °C for
443 18 hours to hydrolyze the proteins. 1mL of chloroform was then added to each sample followed
444 by centrifuge at 400x g for 10 minutes. Supernatants were taken for further preparation. The
445 supernatant was dried by N₂ gas at 37°C. GC-MS method for small polar metabolites assay used
446 in this study was adapted from Wang et al. (2018). The dried residues were resuspended in 25μL
447 methoxylamine hydrochloride (2%(w/v) in pyridine) and incubated at 40°C for 90 minutes. 35
448 μL of MTBSTFA + 1% TBDMS was then added, followed by 30-minute incubation at 60°C.
449 The supernatants from proline tracing experiments were dried by N₂ gas at 37°C followed by
450 resuspension in 50 μL of MTBSTFA + 1% TBDMS incubated at 60 °C for 30 minutes. The
451 derivatized sampled were centrifuged for 5 minutes at 10000x g force. Supernatant from each
452 sample was transferred to GC vials for analysis. 1μL of each sample was injected in split or
453 splitless mode depending on analyte of interest. GC oven temperature was set at 80 °C for 2

454 minutes, increased to 280 °C at a rate of 7 °C/min, and then kept at 280 °C for a total run time of
455 40 minutes.

456 GC-MS analysis was performed on an Agilent 7890B GC system equipped with a HP-5MS
457 capillary column (30 m, 0.25 mm i.d., 0.25 mm-phase thickness; Agilent J&W Scientific),
458 connected to an Agilent 5977A Mass Spectrometer operating under ionization by electron impact
459 (Meister, 1975) at 70 eV. Helium flow was maintained at 1 mL/min. The source temperature was
460 maintained at 230 °C, the MS quad temperature at 150 °C, the interface temperature at 280 °C,
461 and the inlet temperature at 250 °C. Mass spectra were recorded in selected ion monitoring (SIM)
462 mode with 4 ms dwell time.

463

464 **Amino acid uptake assay**

465 Amino acid uptake assays were performed as previously described (Shen & Karner, 2021). Cells
466 were first washed three times with PBS and incubated with Krebs Ringer Hepes (KRH) (120mM
467 NaCl, 5mM KCl, 2mM CaCl₂, 1mM MgCl₂, 25mM NaHCO₃, 5mM HEPES, 1mM D-Glucose)
468 with 4μCi/mL L-[2,3,4-³H]-Proline (PerkinElmer NET323250UC), L-[3,4-³H]-Glutamine
469 (PerkinElmer NET551250UC), L-[2,3-³H]-Alanine (PerkinElmer NET348250UC), L-[1,2-¹⁴C]-
470 Alanine (PerkinElmer NEC266E050UC) , L-[³H(G)]-Serine (PerkinElmer NET248250UC), L-
471 [¹⁴C(U)]-Glycine (PerkinElmer NEC276E050UC), or L-[3,4-³H]-Glutamate (PerkinElmer
472 NET490001MC) for 5 minutes at 37°C. Uptake and metabolism were terminated with ice cold
473 KRH and the cells were scraped with 1% SDS. Cell lysates were combined with 8mL Ultima
474 Gold scintillation cocktail (PerkinElmer 6013329) and CPM was measured using Beckman
475 LS6500 Scintillation counter. Newborn mouse humeri and femurs were used for *ex vivo* amino
476 acid uptake acid. Extemporaneous and cartilaginous tissues were removed from the bones and

477 counter lateral parts were harvested and boiled for normalization. Bones were then incubated
478 with KRH containing radiolabeled amino acids for 30min at 37°C. Uptake and metabolism were
479 terminated by ice cold KRH. Samples were homogenized in RIPA lysis buffer (50 mM Tris (pH
480 7.4), 15 mM NaCl, 0.5% NP-40, 0.1% SDS, 0.1% sodium deoxycholate) followed by sonication
481 using an Ultrasonic Processor (VCX130) (Amplitude: 35%, Pulse 1s, Duration: 10s) and
482 centrifugation. Supernatant from each sample was combined with 8mL scintillation cocktail and
483 CPM was measured using Beckman LS6500 Scintillation counter. Radioactivity was normalized
484 with the boiled contralateral bones.

485

486 **Proline incorporation assay**

487 Cells were incubated with KRH supplemented with 4μCi/mL L-[2,3,4-³H]-Proline for three
488 hours. Cells were lysed with RIPA and followed by centrifugation. Protein is precipitated with
489 TCA and resuspended using 1mL 1M NaOH. 200uL of the dissolved sample was saved for
490 radioactivity reading later as the total proteins. The rest of each sample was split into two: one
491 was treated with 15mg Collagenase P and 60mM HEPES to digest collagens and the other with
492 only 60mM HEPES as the baseline control. Samples were incubated at 37°C for 3hours. After
493 incubation, residual proteins and Collagenase P was precipitated using TCA followed by
494 centrifugation. Supernatant from each sample was combined with 8mL scintillation cocktail and
495 CPM was measured using Beckman LS6500 Scintillation counter. Radioactivity for collagen
496 incorporation was normalized with 60mM HEPES treated the baseline control.

497

498 **RNA isolation and qPCR**

499 Total RNA was harvested from calvarial osteoblasts using TRIZOL and purified by mixing with
500 chloroform. 500ng of total RNA was used for reverse transcription by IScript cDNA synthesis
501 kit (Bio-Rad). SsoAdvanced Universal SYBR Green Supermix (Bio-Rad) was used for qPCR
502 with primers used at 0.1 μ M (listed in Table S3). Technical and biological triplicates were
503 performed using a 96-well plate on an ABI QuantStudio 3. The PCR program was set as 95°C for
504 3min followed by 40 cycles of 95°C for 10s and 60°C for 30s. *Actb* mRNA level was used to
505 normalize expression of genes of interest and relative expression was calculated using the $2^{-(\Delta\Delta Ct)}$
506 method. PCR efficiency was optimized and melting curve analyses of products were performed
507 to ensure reaction specificity.

508

509 **RNAseq**

510 RNA sequencing was performed in biological triplicate by the Duke University Center for
511 Genomic and Computational Biology Sequencing and Genomic Technology Shared Resource on
512 10mg of RNA isolated from primary calvarial cells cultured in either growth or osteogenic media
513 for 7 days. RNA-seq data was processed using the TrimGalore toolkit¹ which employs
514 Cutadapt² to trim low-quality bases and Illumina sequencing adapters from the 3' end of the
515 reads. Only reads that were 20nt or longer after trimming were kept for further analysis. Reads
516 were mapped to the GRCm38v68 version of the mouse genome and transcriptome³ using the
517 STAR RNA-seq alignment tool⁴. Reads were kept for subsequent analysis if they mapped to a
518 single genomic location. Gene counts were compiled using the HTSeq tool⁵. Only genes that had
519 at least 10 reads in any given library were used in subsequent analysis. Normalization and
520 differential expression were carried out using the DESeq2⁶ Bioconductor⁷ package with the R
521 statistical programming environment⁸. The false discovery rate was calculated to control for

522 multiple hypothesis testing. Gene set enrichment analysis⁹ was performed to identify
523 differentially regulated pathways and gene ontology terms for each of the comparisons
524 performed.

525

526 **Western blotting**

527 Calvarial osteoblasts were scraped in RIPA lysis buffer with cOmplete protease inhibitor and
528 PhosSTOP cocktail tablets (Roche). Protein concentration was determined by BCA protein assay
529 kit (Thermo). Protein (6-20 μ g) was loaded on 4%-15% or 12% polyacrylamide gel and
530 transferred onto Immuno-Blot PVDF membrane. The membranes were blocked for 1 hour at
531 room temperature in 5% milk powder in TBS with 0.1% Tween (TBST) and then incubated at
532 4°C with the primary antibody overnight. Primary antibodies were used at 1:1000 to detect
533 proteins, listed as follows: Anti-SNAT2 (AB_2050321), Anti-P-S240/244 S6 (AB_331682),
534 Anti-S6 (AB_331355), Anti-P-S51 Eif2a (AB_2096481), Anti-Eif2a (AB_10692650), Anti-
535 Colla1 (AB_1672342), Anti-Runx2 (AB_10949892), Anti- β -actin (AB_330288), Anti-Smad1
536 (AB_2107780), Anti-4E-BP1 (AB_2097841), Anti-ATF4 (AB_2058752), Anti-mTOR
537 (AB_2105622), Anti-Akt (AB_329827), Anti-Erk (AB_390779), Anti-eEF2 (AB_10693546),
538 Anti-Phgdh (AB_2750870), Anti- α -Tubulin (AB_2619646), Anti-Osx (AB_2895257).
539 Membranes were then incubated at room temperature with Anti-Rabbit IgG (AB_2099233) or
540 Anti-Mouse IgG, HRP-linked Antibody (AB_330924) at 1:2000 for 1 hour at room temperature.
541 Immunoblots were next developed by enhanced chemiluminescence (Clarity Substrate Kit or
542 SuperSignal West Femto substrate). Each experiment was repeated with at least three
543 independently prepared protein extractions. Densitometry was performed for quantification for
544 each blot.

545

546 **Amino acid proportion and amino acid demand prediction analysis**

547 Amino acid sequences of proteins (Mus_musculus.GRCm38.pep.all.fa)

548 were retrieved from Ensembl (<https://uswest.ensembl.org/info/data/ftp/index.html>). Amino acid

549 proportion was calculated based on the amino acid sequences of specific proteins (RUNX2,

550 COL1A1, OSX and OCN) and proteins associated with different GO terms. mRNA expression

551 of genes in undifferentiated and differentiated osteoblasts were obtained from transcriptomic

552 analysis. Top 500 induced and suppressed genes from differentiated osteoblasts were selected for

553 the calculation of proline proportion. For amino acid demand prediction, amino acid proportion

554 and mRNA expression were merged using *Gene.stable.ID* as the bridge. 75 unmatched proteins

555 were excluded from a total of 49665 proteins. To predict the amino acid demand change,

556 changes in mRNA expression was assumed to be proportional to changes in protein translation.

557 Based on this, the change of amino acid demand in each protein is proportional to mRNA

558 expression change:

$$\begin{aligned}\Delta AA &\propto \Delta R \times N_{aa} \\ AA &= \text{amino acid demand} \\ R &= \text{mRNA abundance}\end{aligned}$$

559 N_{aa} = number of amino acids

560 To summarize the overall change of amino acid demand during osteoblast differentiation:

$$\% \Delta AA = \frac{\sum[(R_{differentiated} - R_{undifferentiated}) \times N_{aa}]}{\sum[R_{undifferentiated} \times N_{aa}]} \times 100\%$$

561

562 **tRNA aminoacylation assay**

563 The method is adapted from (Loayza-Puch et al., 2016; Saikia et al., 2016). Purified RNA was

564 resuspended in 30mM NaOAc/HOAc (pH 4.5). RNA was divided into two parts (2 μ g each): one

565 was oxidized with 50mM NaIO₄ in 100mM NaOAc/HOAc (pH 4.5) and the other was treated

566 with 50mM NaCl in NaOAc/HOAc (pH 4.5) for 15 min at room temperature. Samples were
567 quenched with 100mM glucose for 5min at room temperature, followed by desalting using G50
568 columns and precipitation using ethanol. tRNA was then deacylated in 50mM Tris-HCl (pH 9)
569 for 30min at 37°C, followed by another ethanol precipitation. RNA (400ng) was then ligated the
570 3'adaptor (5'-/5rApp/TGGAATTCTCGGGTGCCAAGG/3ddC/-3') using T4 RNA ligase 2
571 (NEB) for 4 h at 37°C. 1µg RNA was then reverse transcribed using SuperScript III first strand
572 synthesis system with the primer (GCCTTGGCACCCGAGAATTCCA) following the
573 manufacturer's instruction. Relative charging level was calculated by qRT-PCR using tRNA-
574 specific primers stated in Table S2.

575

576 **Flow Cytometry**

577 Flow cytometry was used to analyze EdU incorporation and cell viability in calvarial osteoblasts.
578 EdU incorporation was performed using Click-iT™ EdU Alexa Fluor™ 488 Flow Cytometry
579 Assay Kit. Cell were incubated with EdU (5-ethynyl-2'-deoxyuridine, 10 µM) for 24 hours. Cells
580 were then trypsinized, fixed, permeabilized and incubated with Click-iT reaction cocktail for 30
581 minutes according to manufacturer's instructions. Cell viability was analyzed using the Cell
582 Meter™ APC-Annexin V Binding Apoptosis Assay Kit (Cat# 22837). Cells were trypsinized
583 and incubated with APC-Annexin V conjugate and propidium iodide for 30min. Cells were all
584 resuspended in 500µL PBS and analyzed using FACSCanto II flow cytometer (BD Biosciences).
585 Data were analyzed and evaluated using FlowJo (v.11).

586

587 **Quantification and Statistical analysis**

588 Statistical analyses were performed using either Graphpad Prism 6 or R software. One-way
589 ANOVA or unpaired 2-tailed Student's t-test were used to determine statistical significance as
590 indicated in the text. All data are shown as mean values \pm SD or SEM as indicated. $p < 0.05$ is
591 considered as statistically significant. Sample size (n) and other statistical parameters are
592 included in the figure legends. Experiments were repeated on a minimum of 3 independent
593 samples unless otherwise noted.
594

595 **Acknowledgements:**

596 The authors thank Drs. Thomas Carroll and Guoli Hu for critical comments on this manuscript.

597 This work was supported by the National Institute of Arthritis and Musculoskeletal and Skin

598 Diseases (NIAMS) grants (AR076325 and AR071967) to C.M.K.

599

600 **Author Contributions**

601 Conceptualization, C.M.K; Investigation, L.S., Y.Y., Y.Z. S.P.M., G.Z., and C.M.K.; Writing –

602 Original Draft, L.S.; Writing – Review & Editing, G.Z. and C.M.K.; Supervision, C.M.K.

603

604

605 **Conflict of Interests**

606 The authors declare no conflicting interests.

607

608

609 **References**

- 610
611 Adamson, L. F., & Ingbar, S. H. (1967). Some properties of the stimulatory effect of thyroid
612 hormones on amino acid transport by embryonic chick bone. *Endocrinology*, *81*(6),
613 1372-1378. doi:10.1210/endo-81-6-1372
- 614 Alves, R. D. A. M., Eijken, M., Swagemakers, S., Chiba, H., Titulaer, M. K., Burgers, P. C., . . . van
615 Leeuwen, J. P. T. M. (2010). Proteomic Analysis of Human Osteoblastic Cells: Relevant
616 Proteins and Functional Categories for Differentiation. *Journal of Proteome Research*,
617 *9*(9), 4688-4700. doi:10.1021/pr100400d
- 618 Baek, W. Y., Park, S. Y., Kim, Y. H., Lee, M. A., Kwon, T. H., Park, K. M., . . . Kim, J. E. (2013).
619 Persistent low level of osterix accelerates interleukin-6 production and impairs
620 regeneration after tissue injury. *PLoS One*, *8*(7), e69859.
621 doi:10.1371/journal.pone.0069859
- 622 Bardai, G., Lemyre, E., Moffatt, P., Palomo, T., Glorieux, F. H., Tung, J., . . . Rauch, F. (2016).
623 Osteogenesis Imperfecta Type I Caused by COL1A1 Deletions. *Calcified Tissue*
624 *International*, *98*(1), 76-84. doi:10.1007/s00223-015-0066-6
- 625 Baum, B. J., & Shteyer, A. (1987). Characteristics of a neutral amino acid transport system
626 (system A) in osteoblastic rat osteosarcoma cells. *Exp Cell Res*, *169*(2), 453-457.
627 doi:10.1016/0014-4827(87)90205-9
- 628 Ben Amor, I. M., Roughley, P., Glorieux, F. H., & Rauch, F. (2013). Skeletal clinical characteristics
629 of osteogenesis imperfecta caused by haploinsufficiency mutations in COL1A1. *Journal*
630 *of Bone and Mineral Research*, *28*(9), 2001-2007. doi:<https://doi.org/10.1002/jbmr.1942>
- 631 Berendsen, A. D., & Olsen, B. R. (2015). Bone development. *Bone*, *80*, 14-18.
632 doi:10.1016/j.bone.2015.04.035
- 633 Bianco, P., Fisher, L. W., Young, M. F., Termine, J. D., & Robey, P. G. (1991). Expression of bone
634 sialoprotein (BSP) in developing human tissues. *Calcif Tissue Int*, *49*(6), 421-426.
635 doi:10.1007/BF02555854
- 636 Bröer, A., Rahimi, F., & Bröer, S. (2016). Deletion of amino acid transporter ASCT2 (SLC1A5)
637 reveals an essential role for transporters SNAT1 (SLC38A1) and SNAT2 (SLC38A2) to
638 sustain glutaminolysis in cancer cells. *Journal of biological chemistry*, *291*(25), 13194-
639 13205.
- 640 Buttgerit, F., & Brand, M. D. (1995). A hierarchy of ATP-consuming processes in mammalian
641 cells. *Biochem J*, *312* (Pt 1)(Pt 1), 163-167. doi:10.1042/bj3120163
- 642 Chen, J., & Long, F. (2018). mTOR signaling in skeletal development and disease. *Bone Research*,
643 *6*(1), 1. doi:10.1038/s41413-017-0004-5
- 644 Choi, J. Y., Pratap, J., Javed, A., Zaidi, S. K., Xing, L., Balint, E., . . . Stein, G. S. (2001). Subnuclear
645 targeting of Runx/Cbfa/AML factors is essential for tissue-specific differentiation during
646 embryonic development. *Proc Natl Acad Sci U S A*, *98*(15), 8650-8655.
647 doi:10.1073/pnas.151236498
- 648 Ducy, P., Desbois, C., Boyce, B., Pinero, G., Story, B., Dunstan, C., . . . Karsenty, G. (1996).
649 Increased bone formation in osteocalcin-deficient mice. *Nature*, *382*(6590), 448-452.
650 doi:10.1038/382448a0

- 651 Ducy, P., Zhang, R., Geoffroy, V., Ridall, A. L., & Karsenty, G. (1997). Osf2/Cbfa1: a
652 transcriptional activator of osteoblast differentiation. *Cell*, *89*(5), 747-754.
653 doi:10.1016/s0092-8674(00)80257-3
- 654 Elefteriou, F., Benson, M. D., Sowa, H., Starbuck, M., Liu, X., Ron, D., . . . Karsenty, G. (2006).
655 ATF4 mediation of NF1 functions in osteoblast reveals a nutritional basis for congenital
656 skeletal dysplasias. *Cell Metab*, *4*(6), 441-451. doi:10.1016/j.cmet.2006.10.010
- 657 Esen, E., Chen, J., Karner, C. M., Okunade, A. L., Patterson, B. W., & Long, F. (2013). WNT-LRP5
658 signaling induces Warburg effect through mTORC2 activation during osteoblast
659 differentiation. *Cell Metab*, *17*(5), 745-755. doi:10.1016/j.cmet.2013.03.017
- 660 Finerman, G. A., & Rosenberg, L. E. (1966). Amino acid transport in bone. Evidence for separate
661 transport systems for neutral amino and imino acids. *J Biol Chem*, *241*(7), 1487-1493.
662 Retrieved from <https://www.ncbi.nlm.nih.gov/pubmed/5946610>
- 663 Grant, M. E., & Prockop, D. J. (1972). The Biosynthesis of Collagen. *New England Journal of*
664 *Medicine*, *286*(4), 194-199. doi:10.1056/NEJM197201272860406
- 665 Grewal, S., Defamie, N., Zhang, X., De Gois, S., Shawki, A., Mackenzie, B., . . . Erickson, J. D.
666 (2009). SNAT2 amino acid transporter is regulated by amino acids of the SLC6 gamma-
667 aminobutyric acid transporter subfamily in neocortical neurons and may play no role in
668 delivering glutamine for glutamatergic transmission. *The Journal of biological chemistry*,
669 *284*(17), 11224-11236. doi:10.1074/jbc.M806470200
- 670 Guntur, A. R., & Rosen, C. J. (2012). Bone as an endocrine organ. *Endocrine practice : official*
671 *journal of the American College of Endocrinology and the American Association of*
672 *Clinical Endocrinologists*, *18*(5), 758-762. doi:10.4158/EP12141.RA
- 673 Hahn, T. J., Downing, S. J., & Phang, J. M. (1969). Amino acid transport in adult diaphyseal bone:
674 contrast with amino acid transport mechanisms in fetal membranous bone. *Biochim*
675 *Biophys Acta*, *183*(1), 194-203. doi:10.1016/0005-2736(69)90143-6
- 676 Hahn, T. J., Downing, S. J., & Phang, J. M. (1971). Insulin effect on amino acid transport in bone:
677 dependence on protein synthesis and Na+. *American Journal of Physiology-Legacy*
678 *Content*, *220*(6), 1717-1723. doi:10.1152/ajplegacy.1971.220.6.1717
- 679 Hoffmann, T. M., Cwiklinski, E., Shah, D. S., Stretton, C., Hyde, R., Taylor, P. M., & Hundal, H. S.
680 (2018). Effects of Sodium and Amino Acid Substrate Availability upon the Expression and
681 Stability of the SNAT2 (SLC38A2) Amino Acid Transporter. *Frontiers in Pharmacology*,
682 *9*(63). doi:10.3389/fphar.2018.00063
- 683 Hollinshead, K. E. R., Munford, H., Eales, K. L., Bardella, C., Li, C., Escribano-Gonzalez, C., . . .
684 Tennant, D. A. (2018). Oncogenic IDH1 Mutations Promote Enhanced Proline Synthesis
685 through PYCR1 to Support the Maintenance of Mitochondrial Redox Homeostasis. *Cell*
686 *Rep*, *22*(12), 3107-3114. doi:10.1016/j.celrep.2018.02.084
- 687 Hu, G., Yu, Y., Tang, Y. J., Wu, C., Long, F., & Karner, C. M. (2020). The Amino Acid Sensor
688 Eif2ak4/GCN2 Is Required for Proliferation of Osteoblast Progenitors in Mice. *Journal of*
689 *Bone and Mineral Research*, *35*(10), 2004-2014. doi:<https://doi.org/10.1002/jbmr.4091>
- 690 Jagannathan-Bogdan, M., & Zon, L. I. (2013). Hematopoiesis. *Development (Cambridge,*
691 *England)*, *140*(12), 2463-2467. doi:10.1242/dev.083147
- 692 Kandasamy, P., Gyimesi, G., Kanai, Y., & Hediger, M. A. (2018). Amino acid transporters revisited:
693 New views in health and disease. *Trends Biochem Sci*, *43*(10), 752-789.
694 doi:10.1016/j.tibs.2018.05.003

- 695 Karner, C. M., Esen, E., Okunade, A. L., Patterson, B. W., & Long, F. (2015). Increased glutamine
696 catabolism mediates bone anabolism in response to WNT signaling. *J Clin Invest*, *125*(2),
697 551-562. doi:10.1172/JCI78470
- 698 Kern, B., Shen, J., Starbuck, M., & Karsenty, G. (2001). Cbfa1 contributes to the osteoblast-
699 specific expression of type I collagen genes. *J Biol Chem*, *276*(10), 7101-7107.
700 doi:10.1074/jbc.M006215200
- 701 Komori, T., Yagi, H., Nomura, S., Yamaguchi, A., Sasaki, K., Deguchi, K., . . . Kishimoto, T. (1997).
702 Targeted disruption of Cbfa1 results in a complete lack of bone formation owing to
703 maturational arrest of osteoblasts. *Cell*, *89*(5), 755-764. doi:10.1016/s0092-
704 8674(00)80258-5
- 705 Krane, S. M. (2008). The importance of proline residues in the structure, stability and
706 susceptibility to proteolytic degradation of collagens. *Amino Acids*, *35*(4), 703-710.
707 doi:10.1007/s00726-008-0073-2
- 708 Lapunzina, P., Aglan, M., Temtamy, S., Caparrós-Martín, J. A., Valencia, M., Letón, R., . . . Ruiz-
709 Perez, V. L. (2010). Identification of a frameshift mutation in Osterix in a patient with
710 recessive osteogenesis imperfecta. *Am J Hum Genet*, *87*(1), 110-114.
711 doi:10.1016/j.ajhg.2010.05.016
- 712 Lee, B., Thirunavukkarasu, K., Zhou, L., Pastore, L., Baldini, A., Hecht, J., . . . Karsenty, G. (1997).
713 Missense mutations abolishing DNA binding of the osteoblast-specific transcription
714 factor OSF2/CBFA1 in cleidocranial dysplasia. *Nat Genet*, *16*(3), 307-310.
715 doi:10.1038/ng0797-307
- 716 Lee, W.-C., Ji, X., Nissim, I., & Long, F. (2020). Malic Enzyme Couples Mitochondria with Aerobic
717 Glycolysis in Osteoblasts. *Cell Reports*, *32*(10), 108108.
718 doi:<https://doi.org/10.1016/j.celrep.2020.108108>
- 719 Liu, W., Glunde, K., Bhujwalla, Z. M., Raman, V., Sharma, A., & Phang, J. M. (2012). Proline
720 oxidase promotes tumor cell survival in hypoxic tumor microenvironments. *Cancer Res*,
721 *72*(14), 3677-3686. doi:10.1158/0008-5472.CAN-12-0080
- 722 Liu, W., Le, A., Hancock, C., Lane, A. N., Dang, C. V., Fan, T. W., & Phang, J. M. (2012).
723 Reprogramming of proline and glutamine metabolism contributes to the proliferative
724 and metabolic responses regulated by oncogenic transcription factor c-MYC. *Proc Natl*
725 *Acad Sci U S A*, *109*(23), 8983-8988. doi:10.1073/pnas.1203244109
- 726 Loayza-Puch, F., Rooijers, K., Buil, L. C., Zijlstra, J., Oude Vrielink, J. F., Lopes, R., . . . Agami, R.
727 (2016). Tumour-specific proline vulnerability uncovered by differential ribosome codon
728 reading. *Nature*, *530*(7591), 490-494. doi:10.1038/nature16982
- 729 Long, F. (2012). Building strong bones: molecular regulation of the osteoblast lineage. *Nature*
730 *Reviews Molecular Cell Biology*, *13*(1), 27-38. doi:10.1038/nrm3254
- 731 Lou, Y., Javed, A., Hussain, S., Colby, J., Frederick, D., Pratap, J., . . . Stein, J. L. (2009). A Runx2
732 threshold for the cleidocranial dysplasia phenotype. *Human Molecular Genetics*, *18*(3),
733 556-568. doi:10.1093/hmg/ddn383
- 734 Meyer, M. B., Benkusky, N. A., Lee, C. H., & Pike, J. W. (2014). Genomic determinants of gene
735 regulation by 1,25-dihydroxyvitamin D3 during osteoblast-lineage cell differentiation. *J*
736 *Biol Chem*, *289*(28), 19539-19554. doi:10.1074/jbc.M114.578104

- 737 Morotti, M., Bridges, E., Valli, A., Choudhry, H., Sheldon, H., Wigfield, S., . . . Jones, D. (2019).
738 Hypoxia-induced switch in SNAT2/SLC38A2 regulation generates endocrine resistance in
739 breast cancer. *Proceedings of the National Academy of Sciences*, *116*(25), 12452-12461.
740 Mundlos, S., Otto, F., Mundlos, C., Mulliken, J. B., Aylsworth, A. S., Albright, S., . . . Olsen, B. R.
741 (1997). Mutations involving the transcription factor CBFA1 cause cleidocranial dysplasia.
742 *Cell*, *89*(5), 773-779. doi:10.1016/s0092-8674(00)80260-3
743 Nagano, T., Nakashima, A., Onishi, K., Kawai, K., Awai, Y., Kinugasa, M., . . . Kamada, S. (2017).
744 Proline dehydrogenase promotes senescence through the generation of reactive oxygen
745 species. *J Cell Sci*, *130*(8), 1413-1420. doi:10.1242/jcs.196469
746 Nakashima, K., Zhou, X., Kunkel, G., Zhang, Z., Deng, J. M., Behringer, R. R., & de Crombrughe,
747 B. (2002). The novel zinc finger-containing transcription factor osterix is required for
748 osteoblast differentiation and bone formation. *Cell*, *108*(1), 17-29. doi:10.1016/s0092-
749 8674(01)00622-5
750 Otto, F., Thornell, A. P., Crompton, T., Denzel, A., Gilmour, K. C., Rosewell, I. R., . . . Owen, M. J.
751 (1997). Cbfa1, a candidate gene for cleidocranial dysplasia syndrome, is essential for
752 osteoblast differentiation and bone development. *Cell*, *89*(5), 765-771.
753 doi:10.1016/s0092-8674(00)80259-7
754 Phang, J. M. (2019). Proline Metabolism in Cell Regulation and Cancer Biology: Recent Advances
755 and Hypotheses. *Antioxid Redox Signal*, *30*(4), 635-649. doi:10.1089/ars.2017.7350
756 Phang, J. M., Liu, W., Hancock, C., & Christian, K. J. (2012). The proline regulatory axis and
757 cancer. *Front Oncol*, *2*, 60. doi:10.3389/fonc.2012.00060
758 Rached, M. T., Kode, A., Xu, L., Yoshikawa, Y., Paik, J. H., Depinho, R. A., & Kousteni, S. (2010).
759 FoxO1 is a positive regulator of bone formation by favoring protein synthesis and
760 resistance to oxidative stress in osteoblasts. *Cell Metab*, *11*(2), 147-160.
761 doi:10.1016/j.cmet.2010.01.001
762 Rodda, S. J., & McMahon, A. P. (2006). Distinct roles for Hedgehog and canonical Wnt signaling
763 in specification, differentiation and maintenance of osteoblast progenitors.
764 *Development*, *133*(16), 3231-3244. doi:10.1242/dev.02480
765 Saikia, M., Wang, X., Mao, Y., Wan, J., Pan, T., & Qian, S. B. (2016). Codon optimality controls
766 differential mRNA translation during amino acid starvation. *Rna*, *22*(11), 1719-1727.
767 doi:10.1261/rna.058180.116
768 Salhotra, A., Shah, H. N., Levi, B., & Longaker, M. T. (2020). Mechanisms of bone development
769 and repair. *Nature Reviews Molecular Cell Biology*, *21*(11), 696-711.
770 doi:10.1038/s41580-020-00279-w
771 Sanjana, N. E., Shalem, O., & Zhang, F. (2014). Improved vectors and genome-wide libraries for
772 CRISPR screening. *Nat Methods*, *11*(8), 783-784. doi:10.1038/nmeth.3047
773 Sharma, D., Yu, Y., Shen, L., Zhang, G.-F., & Karner, C. M. (2021). SLC1A5 provides glutamine and
774 asparagine necessary for bone development in mice. *eLife*, *10*, e71595.
775 doi:10.7554/eLife.71595
776 Shen, L., & Karner, C. M. (2021). Radiolabeled Amino Acid Uptake Assays in Primary Bone Cells
777 and Bone Explants. In M. J. Hilton (Ed.), *Skeletal Development and Repair: Methods and*
778 *Protocols* (pp. 449-456). New York, NY: Springer US.

- 779 Shen, L., Sharma, D., Yu, Y., Long, F., & Karner, C. M. (2021). Biphasic regulation of glutamine
780 consumption by WNT during osteoblast differentiation. *Journal of Cell Science*, *134*(1).
781 doi:10.1242/jcs.251645
- 782 Stegen, S., Devignes, C. S., Torrekens, S., Van Looveren, R., Carmeliet, P., & Carmeliet, G. (2020).
783 Glutamine Metabolism in Osteoprogenitors Is Required for Bone Mass Accrual and PTH-
784 Induced Bone Anabolism in Male Mice. *J Bone Miner Res*. doi:10.1002/jbmr.4219
- 785 Takarada, T., Nakazato, R., Tsuchikane, A., Fujikawa, K., Iezaki, T., Yoneda, Y., & Hinoi, E. (2016).
786 Genetic analysis of Runx2 function during intramembranous ossification. *Development*,
787 *143*(2), 211-218. doi:10.1242/dev.128793
- 788 Teichmann, L., Chen, C., Hoffmann, T., Smits, S. H. J., Schmitt, L., & Bremer, E. (2017). From
789 substrate specificity to promiscuity: hybrid ABC transporters for osmoprotectants. *Mol*
790 *Microbiol*, *104*(5), 761-780. doi:10.1111/mmi.13660
- 791 Wei, J., Shimazu, J., Makinistoglu, M. P., Maurizi, A., Kajimura, D., Zong, H., . . . Karsenty, G.
792 (2015). Glucose Uptake and Runx2 Synergize to Orchestrate Osteoblast Differentiation
793 and Bone Formation. *Cell*, *161*(7), 1576-1591. doi:10.1016/j.cell.2015.05.029
- 794 Wu, H., Whitfield, T. W., Gordon, J. A. R., Dobson, J. R., Tai, P. W. L., van Wijnen, A. J., . . . Lian, J.
795 B. (2014). Genomic occupancy of Runx2 with global expression profiling identifies a
796 novel dimension to control of osteoblastogenesis. *Genome Biology*, *15*(3), R52.
797 doi:10.1186/gb-2014-15-3-r52
- 798 Yang, X., Matsuda, K., Bialek, P., Jacquot, S., Masuoka, H. C., Schinke, T., . . . Karsenty, G. (2004).
799 ATF4 is a substrate of RSK2 and an essential regulator of osteoblast biology; implication
800 for Coffin-Lowry Syndrome. *Cell*, *117*(3), 387-398. doi:10.1016/s0092-8674(04)00344-7
- 801 Yee, J. A. (1988). Effect of parathyroid hormone on amino acid transport by cultured neonatal
802 mouse calvarial bone cells. *J Bone Miner Res*, *3*(2), 211-218.
803 doi:10.1002/jbmr.5650030214
- 804 Yu, Y., Newman, H., Shen, L., Sharma, D., Hu, G., Mirando, A. J., . . . Karner, C. M. (2019).
805 Glutamine Metabolism Regulates Proliferation and Lineage Allocation in Skeletal Stem
806 Cells. *Cell Metab*, *29*(4), 966-978 e964. doi:10.1016/j.cmet.2019.01.016
- 807 Zhang, A. X., Yu, W. H., Ma, B. F., Yu, X. B., Mao, F. F., Liu, W., . . . Xiang, A. P. (2007). Proteomic
808 identification of differently expressed proteins responsible for osteoblast differentiation
809 from human mesenchymal stem cells. *Mol Cell Biochem*, *304*(1-2), 167-179.
810 doi:10.1007/s11010-007-9497-3
- 811 Zhang, S., Xiao, Z., Luo, J., He, N., Mahlios, J., & Quarles, L. D. (2009). Dose-Dependent Effects of
812 Runx2 on Bone Development. *Journal of Bone and Mineral Research*, *24*(11), 1889-1904.
813 doi:<https://doi.org/10.1359/jbmr.090502>
814
815
816

817 **Figure Legends:**

818 **Figure 1. Osteoblast proteins are enriched with the amino acid proline.**

819 (A) Heat map depicting the relative amino acid enrichment for the indicated osteoblast proteins.

820 Color bar represents fold enrichment relative to the average amino acid content. White boxes
821 denote below average enrichment.

822 (B) Heat map depicting alanine or proline enrichment in differentiation associated proteins.

823 Color bar represents the percent increase in abundance relative to all proteins.

824 (C) Graphical depiction of the proline proportion of the top 500 genes that are induced or
825 suppressed during osteoblast differentiation. Dashed line represents the average proline
826 proportion of all proteins. **** $p \leq 0.00005$. by unpaired 2-tailed Student's t-test.

827 (D) Graphical depiction of the predicted change in demand for alanine or proline based on
828 changes in gene expression during osteoblast differentiation.

829

830 **Figure 2. Proline uptake and incorporation into protein increases during osteoblast**
831 **differentiation.**

832 (A) Graphical depiction of proline, glutamine, glutamate, aspartate, asparagine, serine, glycine
833 and alanine labeling from [U-¹³C]-Proline (n=3), [U-¹³C]-Glutamine (n=3) or [1,2-¹³C]-Glucose
834 (n=3) in naïve calvarial osteoblasts.

835 (B-C) Radiolabeled ³H-Proline uptake assay performed in naive bone marrow stromal cells
836 (BMSC) (B) or after 7 days of osteoblast differentiation (C).

837 (D) Contribution of [U-¹³C]-Proline or [U-¹³C]-Glutamine to proline, glutamate, aspartate,
838 alanine or serine isolated from total protein (n=3).

839 **(E)** Radiolabeled proline incorporation assay performed in primary calvarial cells cultured in
840 growth medium (GM) or osteogenic medium (OM) for 7 days (n=3). ** $p \leq 0.005$, **** $p \leq$
841 0.00005. by unpaired 2-tailed Student's t-test.

842

843 **Figure 3. Proline is essential for the synthesis of proline-enriched osteoblast proteins**

844 **(A)** Western blot analysis of naïve calvarial cells cultured in 0.3mM or 0mM Pro for 48 hours
845 (n=3). In all blots, the percent proline composition is noted under the protein name. Protein
846 expression normalized to total protein. Fold change \pm SD for three independent experiments.

847 **(B)** Correlation analysis of protein expression as a function of the proline composition of
848 proteins in naïve calvarial cells cultured in media containing either 0mM or 0.3mM Pro for 48
849 hours.

850 **(C-G)** The effect of proline availability on the synthesis of select proteins. CHX –
851 cycloheximide. Error bars depict SD. * $p \leq 0.05$. by unpaired 2-tailed Student's t-test.

852

853 **Figure 4. *Slc38a2* provides proline critical for the synthesis of proline-rich proteins.**

854 **(A)** Graphical depiction of the effects of 5mM MEAIB on radiolabeled amino acid uptake in
855 primary calvarial cells (n=3).

856 **(B,C)** Effect of *Slc38a2* targeting on ^3H -Proline uptake (n=5) **(B)**, or protein expression **(C)**. In
857 all blots, the percent proline composition is noted under the protein name Protein expression
858 normalized to total protein. Fold change \pm SD for three independent experiments.

859 **(D)** Correlation analysis of protein expression as a function of the proline composition of
860 proteins in wild type (sgLuc) or *Slc38a2* targeted calvarial cells (sg38a2) calvarial cells. * $p \leq$
861 0.05, *** $p \leq 0.0005$, **** $p \leq 0.00005$. by unpaired 2-tailed Student's t-test.

862

863 **Figure 5. *Slc38a2* dependent proline uptake is required for osteoblast differentiation during**
864 **bone development.**

865 **(A-H)** Skeletal preparations of *Slc38a2*^{LacZ/LacZ} or wildtype controls **(A-B, E-F)** or
866 *Sp7Cre;Slc38a2*^{fl/fl} or *Sp7Cre;Slc38a2*^{fl/+} littermate controls **(C-D, G-H)** at E15.5 **(A-D)** or P1
867 **(E-H)**. Red arrow **(A-D)** or Asterix **(E-H)** highlights reduced mineralization. A total of n=7 or
868 n=5 *Slc38a2*^{LacZ/LacZ} animals and n=5 or n=5 for *Sp7Cre;Slc38a2*^{fl/fl} animals were analyzed at
869 E15.5 or P1 respectively.

870 **(I-R)** Representative von Kossa staining **(I,J)**, alkaline phosphatase (ALPL) staining **(K,L)** *in*
871 *situ* hybridization for *Spp1* **(M,N)**, *Ibsp* **(O,P)**, *Bglap* **(Q,R)** and *Colla1* **(U,V)**, or
872 immunofluorescent staining for OSX **(S',S'',T',T'')** and COL1A1 **(W,X)** on *Sp7Cre;Slc38a2*^{fl/fl}
873 **(J,L,N,P,R,T,V,X)** or *Sp7Cre;Slc38a2*^{fl/+} **(I,K,M,O,Q,S,U,W)** newborn calvariae. *p≤0.05. by
874 paired 2-tailed Student's t-test.

875

876

877

878

879

880

881 **Supplemental Figure Legends**

882 **Figure 1 Supplement 1.**

883 (A) Functional assays of calvarial cells cultured in growth media (GM) or osteogenic medium
884 (OM) for 10 days.

885 (B) qRT-PCR analysis of osteogenic marker genes *Runx2*, *Sp7* (OSX), *Colla1* and *Bglap* in
886 calvarial cells cultured in GM or OM for 7 days (n=3). Error bars depict SD.

887
888 **Figure 2 Supplement 1.**

889 (A,B) Radiolabeled proline or glutamine uptake assay performed in naïve calvarial osteoblasts
890 (A) or after 7 days of osteoblast differentiation (B). Error bars depict SD. ** $p \leq 0.005$, **** $p \leq$
891 0.00005. by unpaired 2-tailed Student's t-test.

892
893 **Figure 3 Supplement 1.**

894 (A) Effect of 48-hour proline withdrawal on tRNA aminoacylation (n=3).
895 (B) Western blot analysis of naïve calvarial cells cultured in 0.3mM or 0mM Pro for 48 hours
896 (n=3). Protein expression normalized to total protein. Phosphorylation normalized to total
897 protein. Fold change \pm SD for three independent experiments.

898 (C) qRT-PCR analysis of the effect of 48-hour proline withdrawal on gene expression in
899 calvarial cells (n=3).

900 (D-F) The effect of proline availability on the synthesis of select proteins. CHX –
901 cycloheximide. Fold change \pm SD for three independent experiments. Error bars depict SD. * $p \leq$
902 0.05. by unpaired 2-tailed Student's t-test.

903
904 **Figure 4 Supplement 1.**

905 (A) Graphical depiction of the effects of 5mM MEAIB on amino acid uptake in humeri or
906 femurs isolated from P3 mice (n=3).

907 (B) Schematic depicting *Slc38a2* Crispr targeting strategy.

908 (C-E) Effect of *Slc38a2* targeting on tRNA aminoacylation (n=3) (C), protein expression (n=3)

909 (D) or mRNA expression (n=3) (E). In all blots, the percent proline composition is noted under

910 the protein name. Protein expression normalized to total protein. Phosphorylation normalized to

911 total protein. Fold change \pm SD for three independent experiments. * $p \leq 0.05$, **** $p \leq 0.00005$.

912 by unpaired 2-tailed Student's t-test.

913

914 **Figure 5 Supplement 1.**

915 (A-D) Effect of *Slc38a2* targeting on cell viability (n=3) (A), EdU incorporation (n=3) (B),

916 mRNA expression (n=3) by qPCR analysis (C), or functional assays (D) in calvarial cells

917 cultured in growth media (GM) or osteogenic medium (OM) for 7 or 10 days. Error bars depict

918 SD. * $p \leq 0.05$. by unpaired 2-tailed Student's t-test.

919

920 **Figure 5 Supplement 2.**

921 (A) Western blot analysis of SNAT2 expression in femurs from *Slc38a2*^{LacZ/LacZ} or wildtype
922 controls. SNAT2 proteins normalized to ACTB.

923 (B) Representative images of humerus skeletal preparations, von Kossa staining, alkaline

924 phosphatase (ALPL) staining, *in situ* hybridization for *Colla1*, or immunofluorescence staining

925 for OSX and COL1A1 on femur sections of E15.5 *Slc38a2*^{LacZ/LacZ} or wildtype controls littermate

926 controls (n=3 animals).

927

928 **Figure 5 Supplement 3.**

929 **(A)** Western blot analysis of SNAT2 expression in femurs from *Sp7Cre;Slc38a2^{fl/fl}* or
930 *Sp7Cre;Slc38a2^{fl/+}* littermate controls. SNAT2 normalized to ACTB.

931 **(B)** Evaluation of amino acid uptake in femurs isolated from newborn *Sp7Cre;Slc38a2^{fl/fl}* or
932 *Sp7Cre;Slc38a2^{fl/+}* littermate controls (n=5).

933 **(C)** Skeletal preparations of newborn *Slc38a2^{LacZ/LacZ}* or wildtype controls (n=5), or
934 *Sp7Cre;Slc38a2^{fl/fl}* or *Sp7Cre;Slc38a2^{fl/+}* littermate controls (n=5). Phalloidin staining or
935 immunofluorescence staining for RUNX2 on P0 *Sp7Cre;Slc38a2^{fl/fl}* or *Sp7Cre;Slc38a2^{fl/+}*
936 calvariae (n=5).

937 **(D)** Representative images of *in situ* hybridization for *Spp1*, *Ibsp*, *Colla1*, and *Sp7*, or
938 immunofluorescence staining for OSX and COL1A1 on humerus sections from E15.5
939 *Sp7Cre;Slc38a2^{fl/fl}* or *Sp7Cre;Slc38a2^{fl/+}* littermate controls (n=5 animals). Fold change \pm SD.

940 Error bar depicts SD. * $p \leq 0.05$, **** $p \leq 0.00005$. by paired 2-tailed Student's t-test.

941

942

943

944 Table 1. Amino acid composition of classical osteoblast proteins.
945

	RUNX2	OSX	COL1A1	OCN	ALL PROTEINS
Ala	0.084	0.082	0.089	0.074	0.068
Cys	0.012	0.026	0.012	0.032	0.023
Asp	0.044	0.033	0.041	0.063	0.048
Glu	0.021	0.044	0.052	0.063	0.069
Phe	0.038	0.023	0.018	0.021	0.038
Gly	0.053	0.138	0.268	0.053	0.063
His	0.028	0.044	0.006	0.000	0.026
Ile	0.021	0.012	0.017	0.042	0.045
Lys	0.031	0.051	0.038	0.063	0.057
Leu	0.059	0.084	0.035	0.147	0.100
Met	0.023	0.012	0.010	0.021	0.023
Asn	0.038	0.026	0.023	0.032	0.036
Pro	0.105	0.133	0.190	0.074	0.061
Gln	0.089	0.033	0.033	0.032	0.048
Arg	0.056	0.040	0.047	0.063	0.056
Ser	0.133	0.098	0.046	0.074	0.085
Thr	0.069	0.056	0.030	0.074	0.054
Val	0.054	0.021	0.029	0.032	0.061
Trp	0.010	0.014	0.004	0.000	0.012
Tyr	0.030	0.030	0.010	0.042	0.027

946

947

948 Table 2. Relative amino acid composition of proteins associated with various differentiated cell types based on GO Terms.

949

	Osteoblast	Epithelial cell	HSC	Endothelial cell	Osteoclast	Neuron	Muscle cell	Cardiomyocyte	All
GO Term	00001649	0030855	0030097	0045446	0030316	0030182	0042692	0055007	
Ala	0.0739	0.0731	0.0695	0.0709	0.0730	0.0728	0.0730	0.0731	0.0681
Cys	0.0301	0.0230	0.0234	0.0259	0.0292	0.0228	0.0233	0.0223	0.0227
Asp	0.0478	0.0483	0.0493	0.0467	0.0468	0.0502	0.0511	0.0490	0.0479
Glu	0.0639	0.0678	0.0671	0.0682	0.0614	0.0693	0.0727	0.0690	0.0694
Phe	0.0331	0.0331	0.0365	0.0342	0.0374	0.0347	0.0367	0.0373	0.0375
Gly	0.0686	0.0698	0.0672	0.0685	0.0656	0.0667	0.0666	0.0667	0.0629
His	0.0273	0.0256	0.0266	0.0239	0.0245	0.0254	0.0249	0.0256	0.0262
Ile	0.0362	0.0401	0.0409	0.0458	0.0407	0.0420	0.0429	0.0441	0.0445
Lys	0.0531	0.0557	0.0570	0.0531	0.0499	0.0560	0.0606	0.0627	0.0571
Leu	0.0946	0.0923	0.0957	0.0950	0.1040	0.0961	0.0930	0.0903	0.1004
Met	0.0220	0.0232	0.0229	0.0224	0.0210	0.0222	0.0222	0.0238	0.0228
Asn	0.0360	0.0361	0.0362	0.0382	0.0366	0.0374	0.0369	0.0363	0.0360
Pro	0.0711	0.0694	0.0659	0.0652	0.0650	0.0644	0.0627	0.0609	0.0612
Gln	0.0469	0.0472	0.0468	0.0458	0.0446	0.0459	0.0464	0.0482	0.0478
Arg	0.0607	0.0573	0.0563	0.0566	0.0539	0.0575	0.0561	0.0547	0.0559
Ser	0.0853	0.0874	0.0848	0.0807	0.0843	0.0835	0.0797	0.0848	0.0853
Thr	0.0527	0.0529	0.0537	0.0557	0.0563	0.0538	0.0528	0.0544	0.0543
Val	0.0568	0.0588	0.0599	0.0639	0.0623	0.0598	0.0599	0.0585	0.0610
Trp	0.0119	0.0110	0.0122	0.0119	0.0135	0.0117	0.0108	0.0105	0.0119
Tyr	0.0278	0.0279	0.0280	0.0275	0.0298	0.0279	0.0275	0.0278	0.0270

950 Table 3. mRNA expression of putative proline transporters.

	System	Alias	cOB FPKM
Slc38a2	A	SNAT2	8823.1
Slc1a4	ASC	ASCT1	3030.7
Slc36a4	LYAAT	PAT4	1929
Slc36a1	LYAAT	PAT1	803.7
Slc38a4	A	SNAT4	267.9
Slc36a2	LYAAT	PAT2	1.1
Slc6a15	B ⁰	B ⁰ AT2	7.5
Slc36a3	LYAAT	PAT3	0
Slc6a7	IMINO ^B	PROT	4.3
Slc6a20a	IMINO	SIT2	0
Slc6a20b	IMINO	SIT1	0
Slc6a19	B ⁰	B ⁰ AT1	0

951

952

953 Table S1. sgRNA protospacer sequence

SP498.mCherry.g17	CAAGTAGTCGGGGATGTCGGNNG
SP498.mCherry.g19	AGTAGTCGGGGATGTCGGCGNNG
SP499.Luc.g3	CAATTCTTTATGCCGGTGTNNG
SP399.Luc.g4	GTGTTGGGCGCGTTATTTATNNG
MS347.Slc38a2.g1	GTATCTGAACGGTGAATATCNGG
MS348.Slc38a2.g11	GAGTTGAAGATGAAATAGCGNNG
MS348.Slc38a2.g13	ATGCCAACGCCAACGCTGCCNNG
MS348.Slc38a2.g21	AAGCAGCTTCCACGGGGCAANGG
MS348.Slc38a2.g4	GTGGCCAACGAACTGTGAANGG

954

955

956

957 Table S2. RT-PCR primer sequences for tRNA charging

Amino acid	tRNA	Primer sequence
Pro	AGG	GGCTCGTTGGTCTAGGGGTATG
Leu	CAG	GTCAGGATGGCCGAGCGGTCTA
Gln	TTG	GGTCCCATGGTGTAAATGGTT
Glu	TTC	CCCACATGGTCTAGCGGTTA
Asn	GTT	GTCTCTGTGGCGCAATCGGT
Val	TAC	GGTTCATAGTGTAGTGGTTAT
Reverse		GCCTTGGCACCCGAGAATTCCA

958

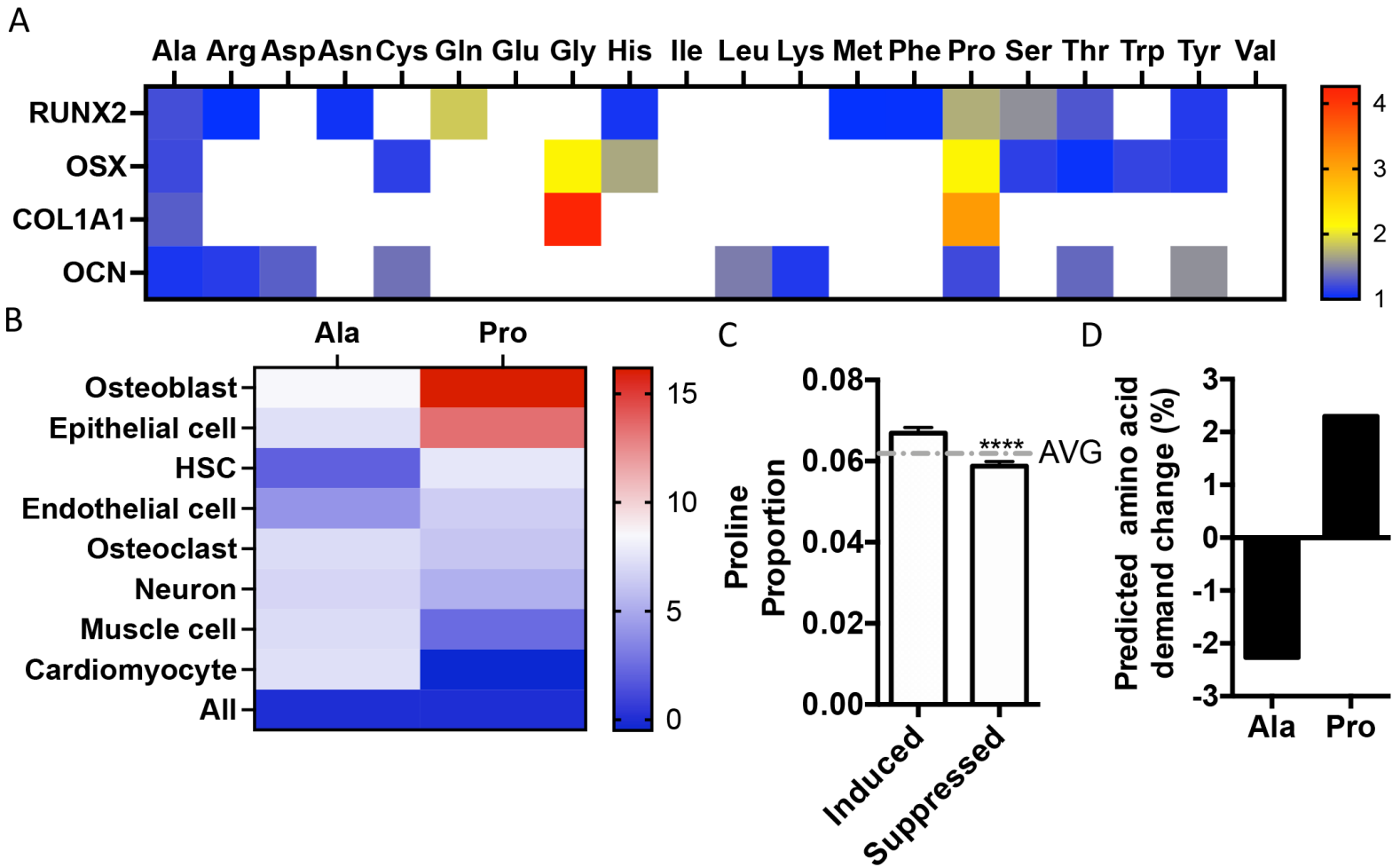
959

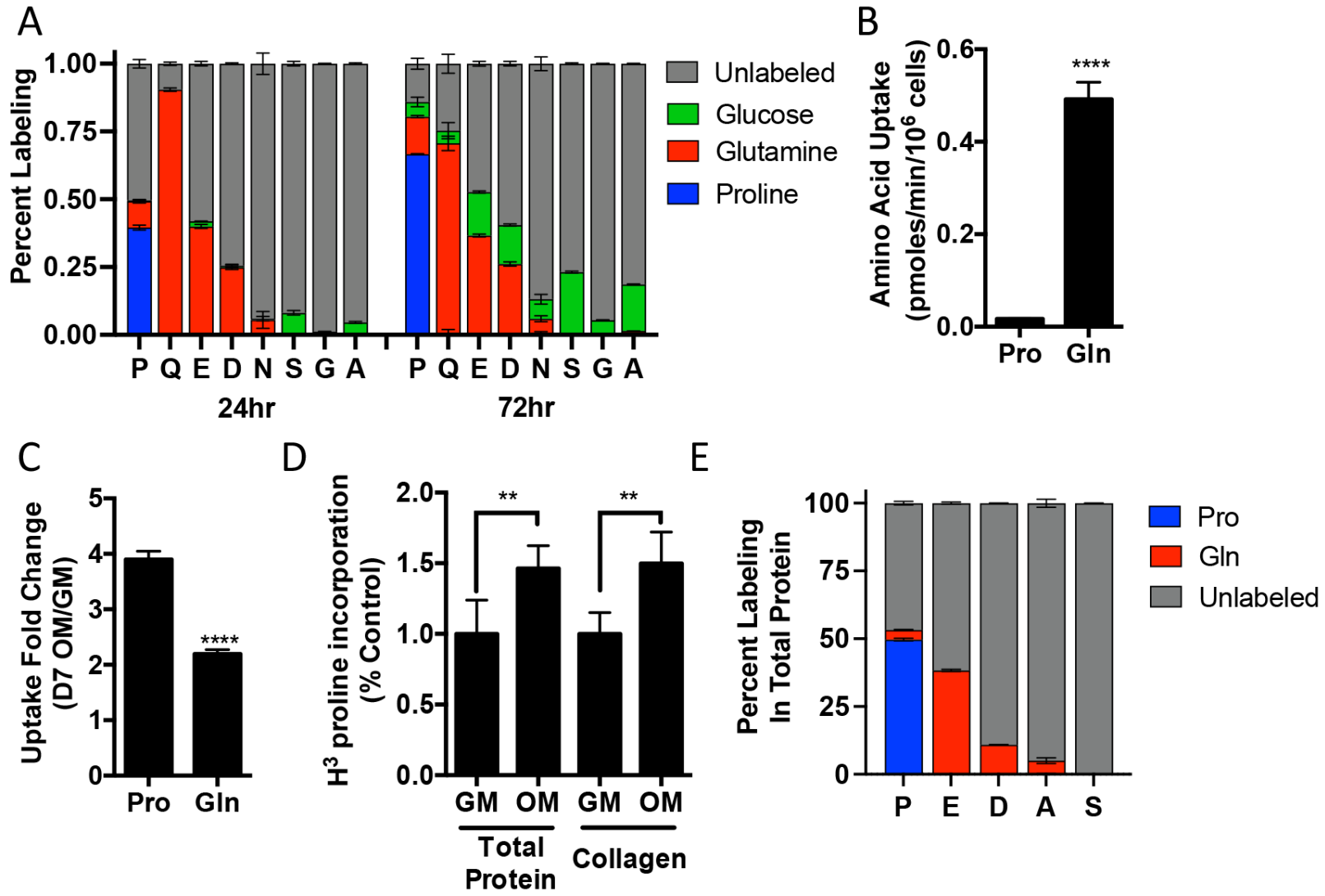
960

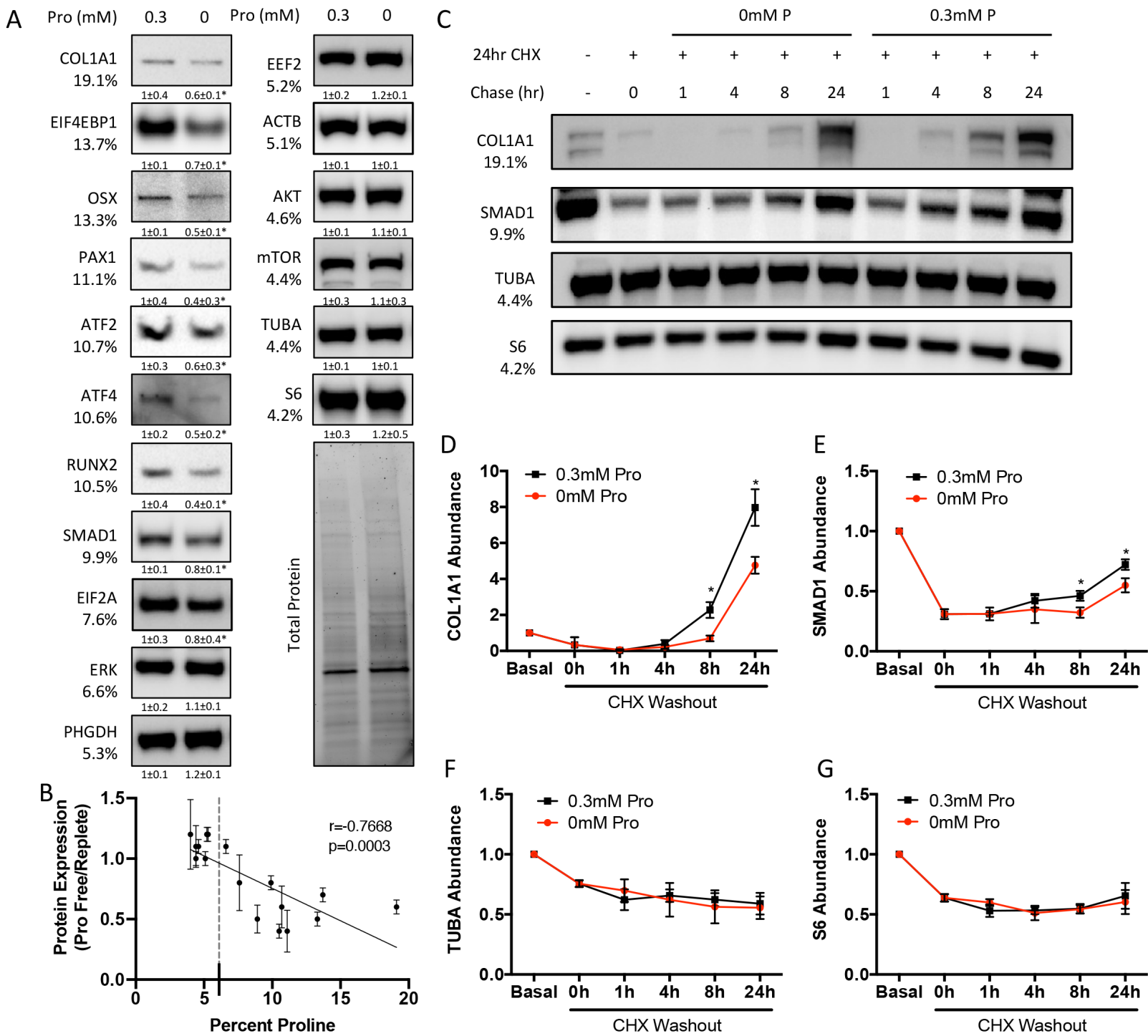
961

962 Table S3. RT-PCR primer sequences

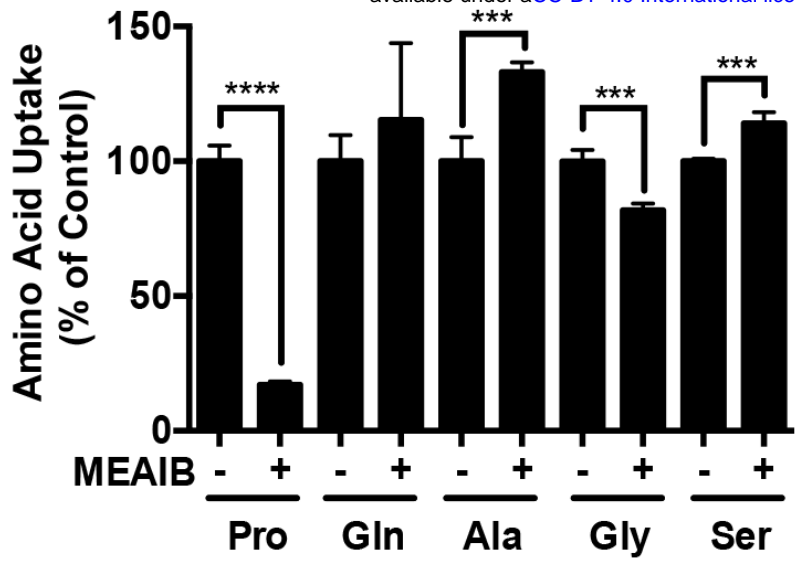
Gene Symbol	Forward	Reverse
β -actin	AGATGTGGATCAGCAAGCAG	GCGCAAGTTAGGTTTTGTCA
Akp2	CCA ACTCTTTTGTGCCAGAGA	GGCTACATTGGTGTGAGCTTTT
Ibsp	CAGAGGAGGCAAGCGTCACT	GCTGTCTGGGTGCCAACACT
Bglap	CAGCGGCCCTGAGTCTGA	GCCGGAGTCTGTTCACCTTA
Sp7	CCCTTCTCAAGCACCAATGG	AAGGGTGGGTAGTCATTTGCATA
Runx2	CCAACCGAGTCATTTAAGGCT	GCTCACGTCGCTCATCTTG
Slc38a2	GGCTATGTCAAGCTACCTCTTC	GTCACCGTTCAGATACCACAA
mTOR	AGAAGGGTCTCCAAGGACGACT	GCAGGACACAAAGGCAGCATTG
Smad1	CTGAAGCCTCTGGAATGCTGTG	CAGAAGGCTGTGCTGAGGATTG
eEF2	CAGAAGTACCGTTGTGAGCTGC	GTCAGAGGTTGGCACCATCTTG
Erk2	TCAAGCCTTCCAACCTCCTGCT	AGCTCTGTACCAACGTGTGGCT
EIF4EBP1	GGAGAGCTGCACAGCATT CAGG	GGAGGTATGTGCTGGTGTTCAC
Akt1	GGACTACTTGCACTCCGAGAAG	CATAGTGGCACCGTCCTTGATC
Phgdh	CCTCCTTTGGTGTTCAGCAGCT	CGCACACCTTTCTTGCACTGAG
Tuba1	GGCAGTGTTTCGTAGACCTGGAA	CTCCTTGCCAATGGTGTAGTGG
Atf4	GCATGCTCTGTTTCGAATGGA	CCAACGTGGTCAAGAGCTCAT
Atf2	CTTCCTCTCCTCAACCAGTCCA	GAGTCCTAACCAATCCACTGCC
Pax1	TCGCCAGCAGTGAATGGACTCG	ATACTCCGTGCTGGTTGGAAGC



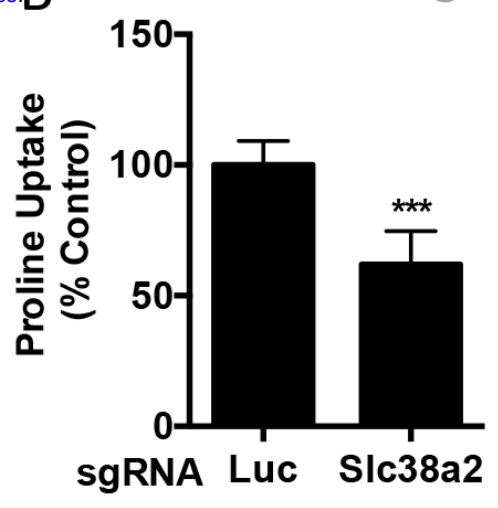




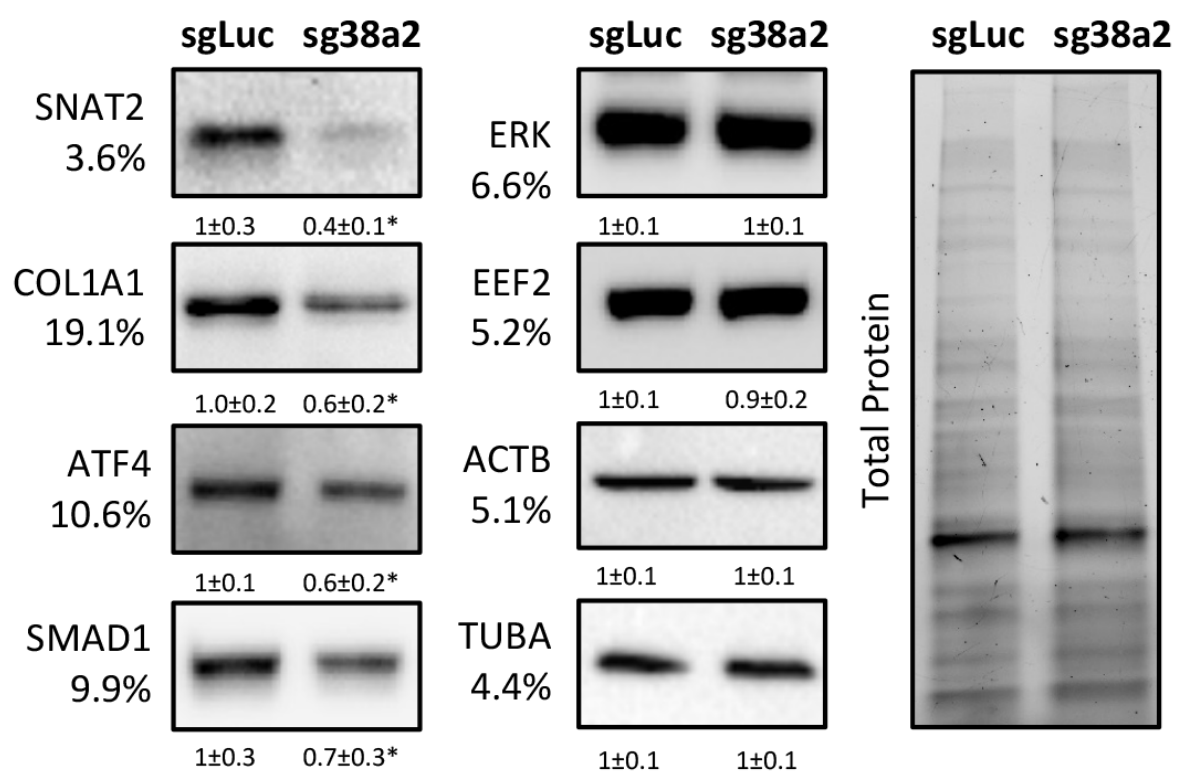
A



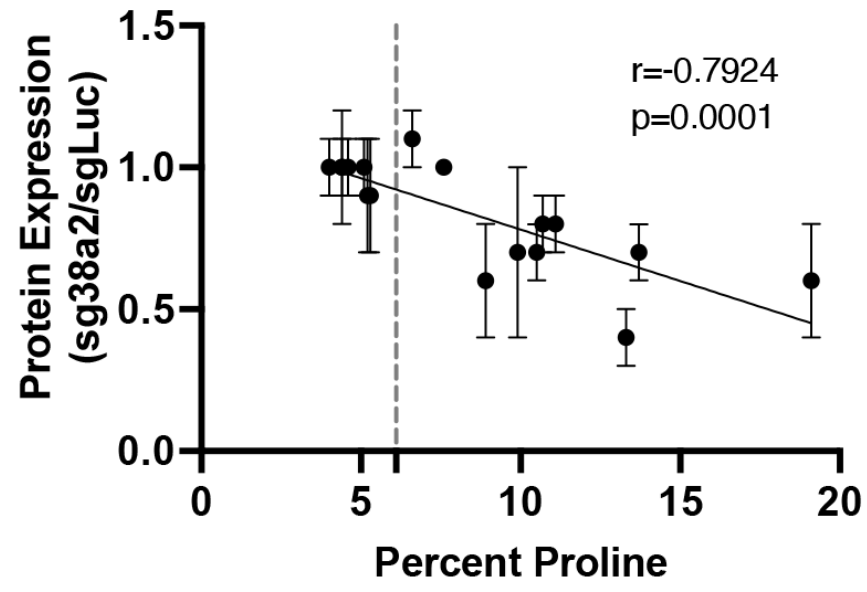
B

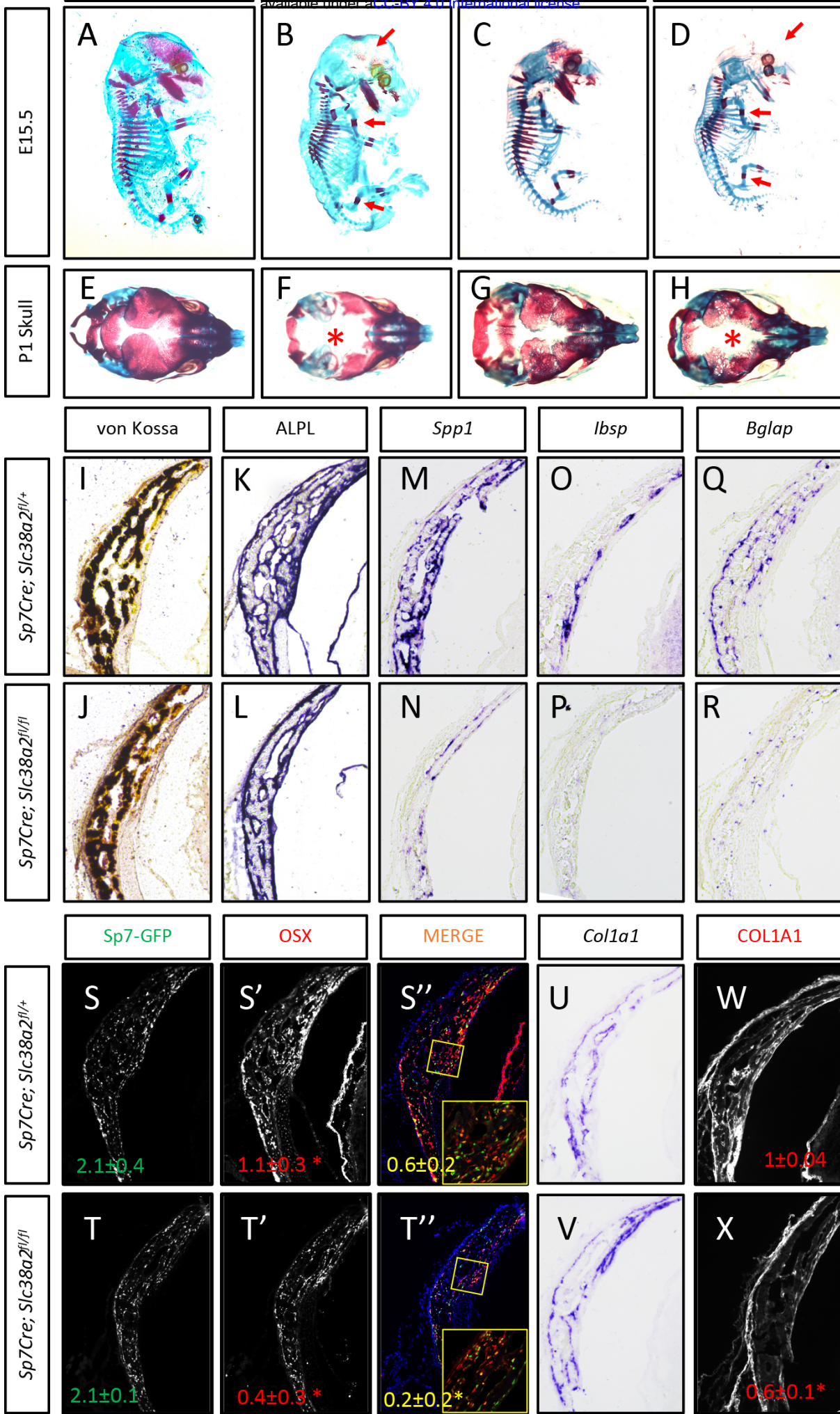


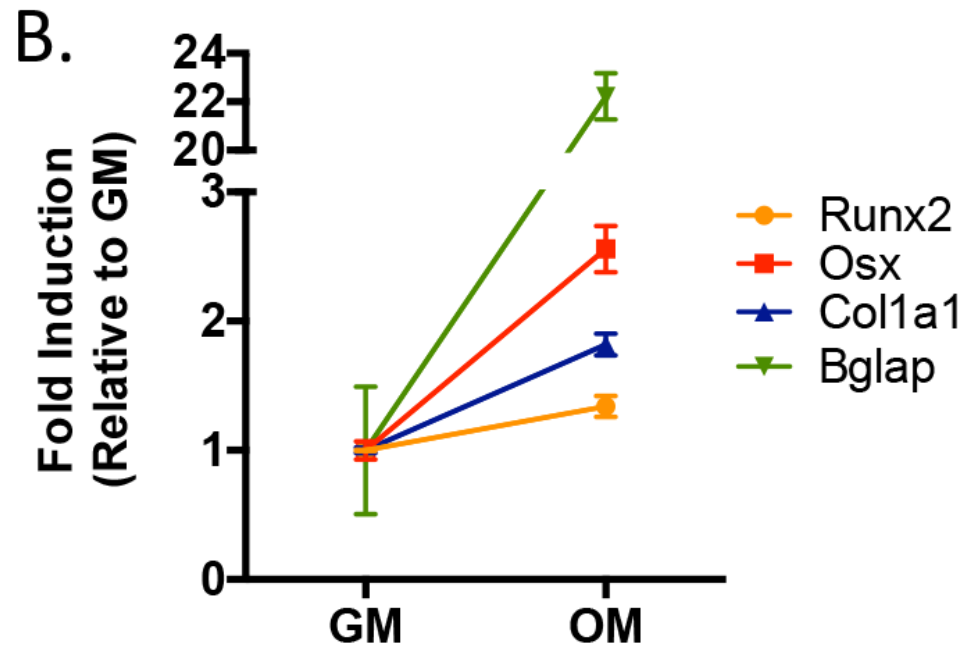
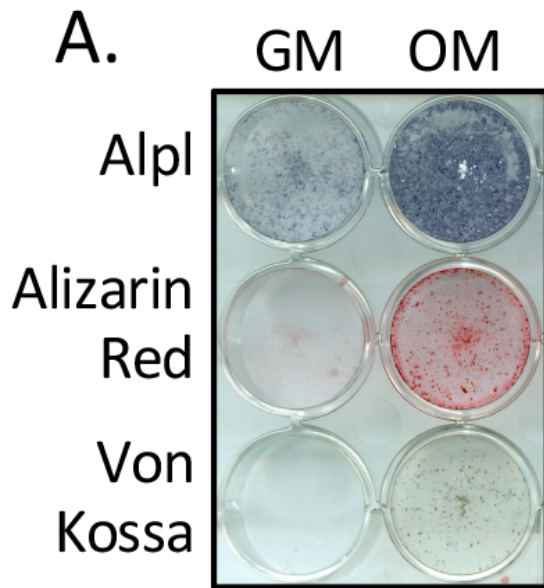
C

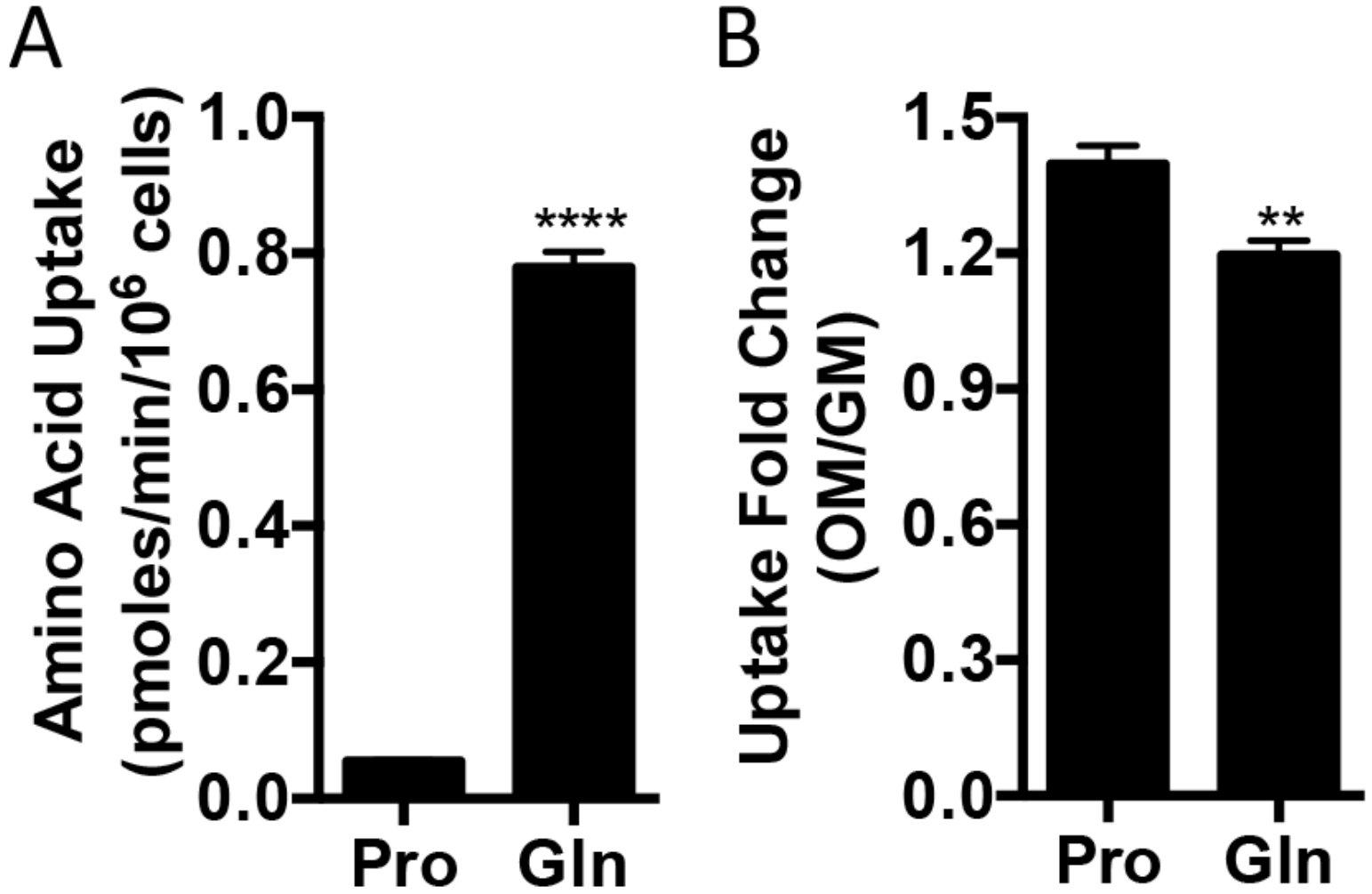


D

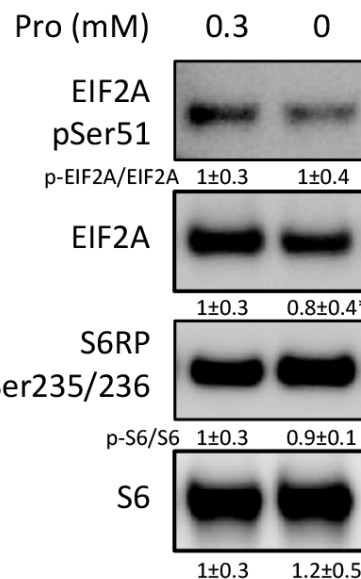
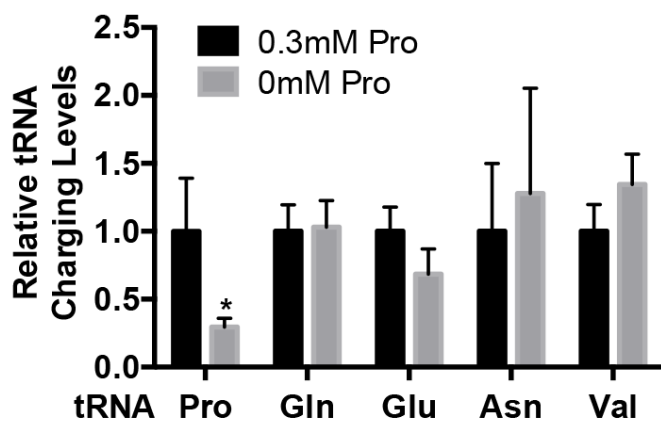




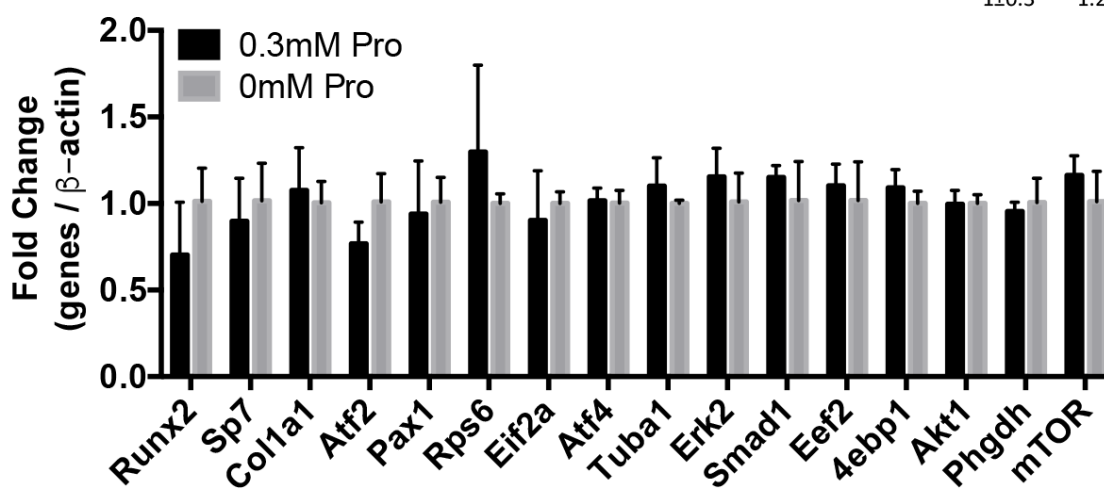




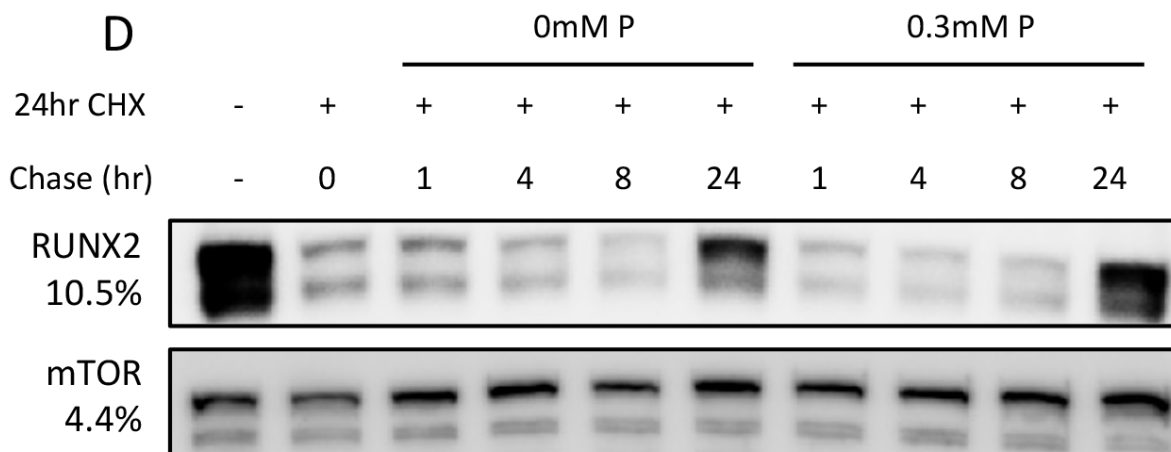
A



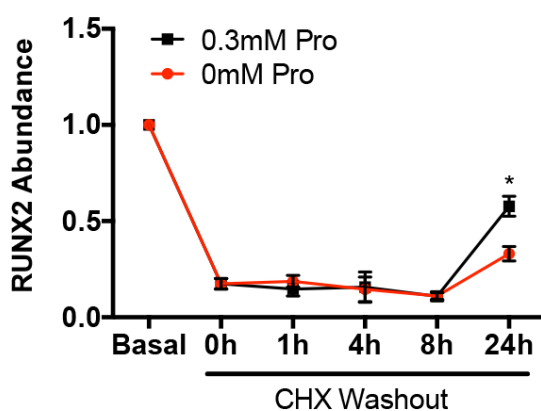
C



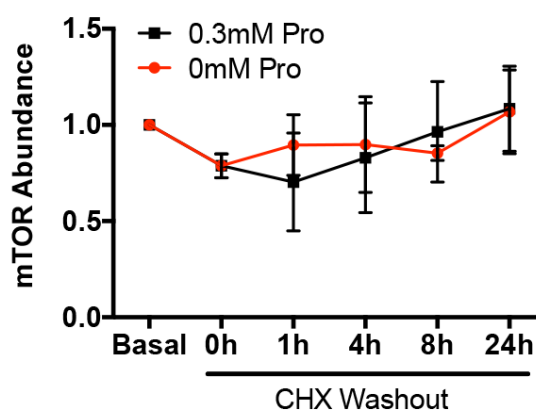
D

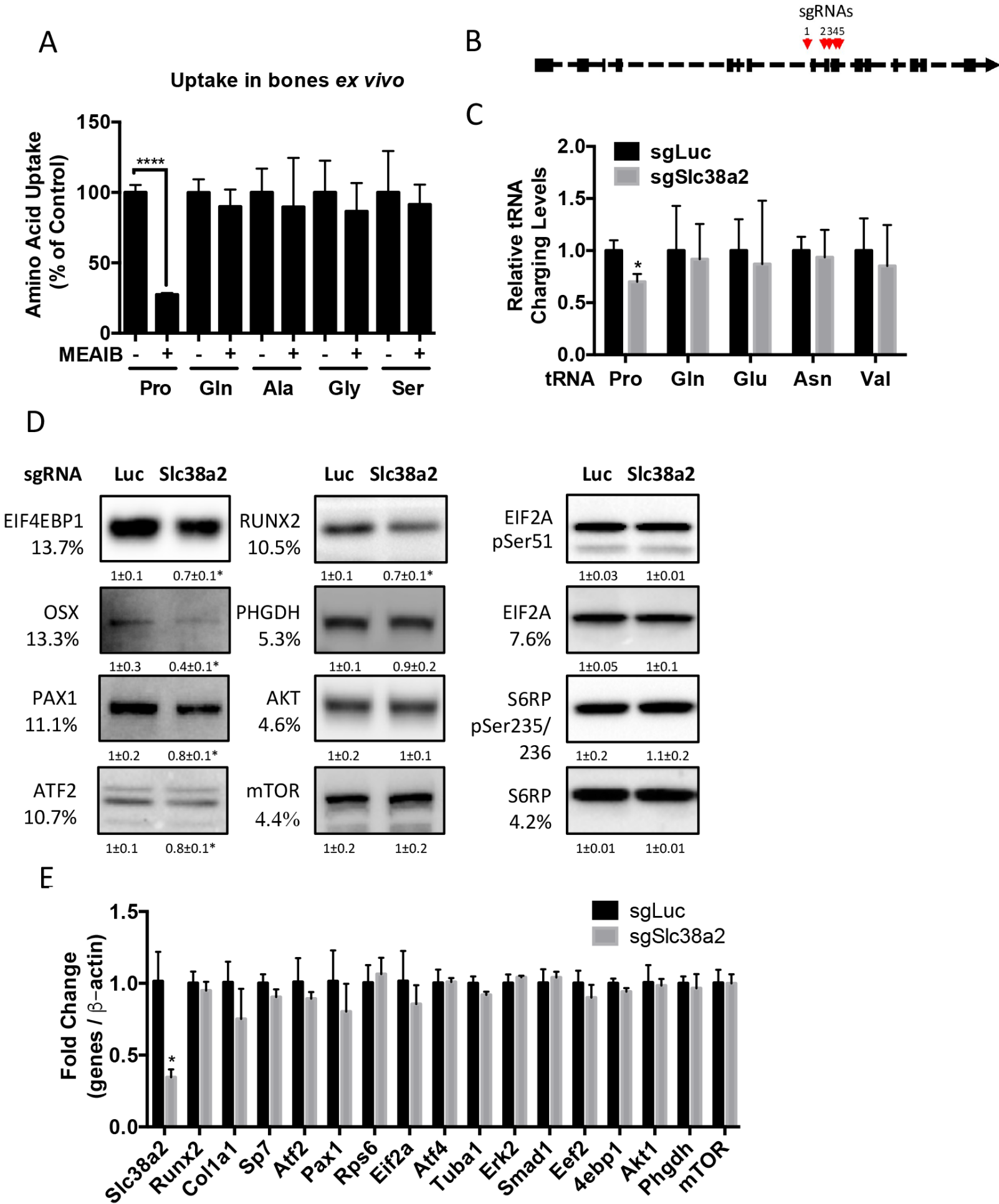


E

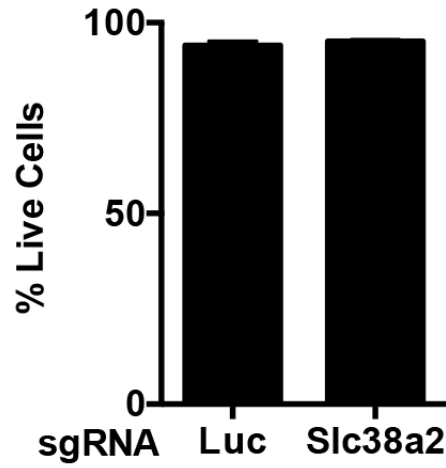


F

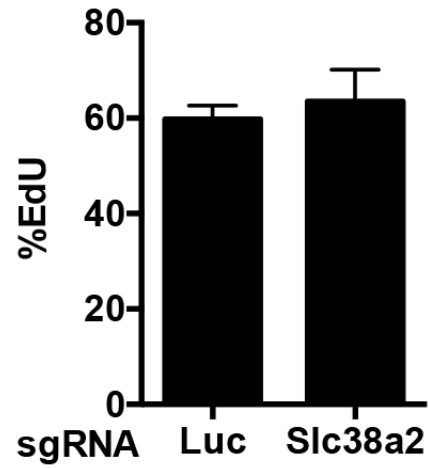




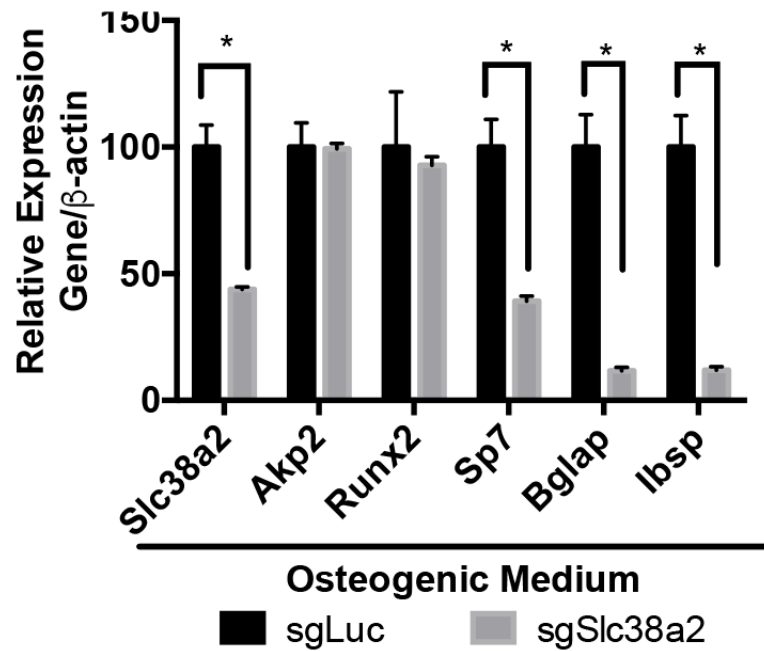
A



B



C



D

